Hochschule für Angewandte Wissenschaften Hamburg
Hamburg University of Applied Sciences

Bachelorarbeit

Jannik Marx

Design concept for a CO_2 vessel safety cooling system

Fakultät Technik und Informatik
Department Maschinenbau und Produktion

Faculty of Engineering and Computer Science
Department of Mechanical Engineering and Production Management

Jannik Marx

Design concept for a CO2 vessel safety cooling system

Bachelorarbeit eingereicht im Rahmen der Bachelorprüfung

im Studiengang Maschinenbau und Produktion
am Department Maschinenbau und Produktion
der Fakultät Technik und Informatik
der Hochschule für Angewandte Wissenschaften Hamburg

in Zusammenarbeit mit:
Europäisches Kernforschungsinstitut (CERN)
Abteilung EP-DT-FS
Espl. des Particules 1
1211 Meyrin
Switzerland

Erstprüfer/in: Prof. Dr. Achim Schmidt
Zweitprüfer/in: Dipl.-Ing. Bart Verlaat

Abgabedatum: 12.03.2024

Zusammenfassung

Jannik Marx

Thema der Bachelorthesis

Konstruktionskonzept eines Sicherheitskühlsystems für einen CO_2-Behälter

Stichworte

CERN, Phase II upgrade, Detektor Kühlung, Kompressionskältemaschine, Transkritische CO_2 Kühlung, Druckverlust, Zweiphasenströmung, Einphasenströmung, Thermosiphon, Ölmanagement, Kryogene Behälter, Wärmeverlustrechnung

Kurzzusammenfassung

Kühlsysteme für Detektoren der künftigen Tracker Detektoren der ATLAS und CMS Experimente des Large Hadron Colliders (LHC) am CERN werden vollständig auf CO2 Kühltechnologie basieren. Das Kühlsystem besteht aus einem zweistufigen transkritischen System und einem Niedertemperatur-Pumpenkreislauf, die beide mit CO_2 betrieben werden. Um die thermischen Anforderungen zu erfüllen, wird ein CO_2-Tank als Systemerweiterung oberhalb des Experiments platziert, da der Platz unter der Erde begrenzt ist. Im Falle eines Ausfalls des Primärsystems muss ein Subsystem einspringen, um den Auslegungsdruck des Tankes aufrechtzuerhalten. In dieser Arbeit wird die Leistung eines Aufbaus, einen handelsüblichen CO2 Verflüssigungssatzes beinhaltend, zum Betrieb eines Wärmetauschers mit deutlichem Höhenunterschied untersucht und die Eignung als redundantes Notkühlsystem. Es wurde eine umfassende Testkampagne durchgeführt, um die Fähigkeit des Systems zu bewerten, unterschiedliche Wärmelasten zu bewältigen. Die Ergebnisse bestätigen die Realisierbarkeit des vorgeschlagenen Notkühlsystems, und es werden Einblicke in seine künftige Umsetzung gegeben.

Title of the paper

Design concept for a CO_2 vessel safety cooling system

Keywords

CERN, Phase II upgrade, Detector cooling, Vapor compression Cycle, Transcritical CO_2 cycle, Pressure drop, Two-phase flow, Single-phase flow, Thermosiphon, Oil management, Cryogenic vessels, Heat leak calculation

Abstract

Detector cooling systems of the future tracking detectors of the ATLAS and CMS experiments at the Large Hadron Collider (LHC) at CERN will be entirely based on CO_2 refrigeration technology. The cooling system consists of a double-stage Transcritical system and a low temperature pumped loop, both operated by CO_2. A storage vessel, located above the experiment accounts for the substantial amount liquid CO_2 required, to fulfil the thermal constraints, due to limited space underground. In the event of a primary system failure, a sub-system must overtake to maintain the vessel's design pressure. This work examines the performance of a setup, containing a commercial condensing unit, to operate a heat exchanger substantially elevated. The suitability as a redundant emergency cooling system is investigated. A comprehensive testing campaign was conducted to assess the system's ability to handle varied heat loads. The findings confirm the viability of the proposed emergency cooling setup and insights to its future implementation are provided.

Contents

List of Figures

List of Tables

Nomenclature

Δh Enthalpy Difference

Δp_{frict} Frictional Pressure Drop

Δp_{mom} Momentum Pressure Drop

Δp_{static} Static Pressure Drop

Δp_{total} Total Pressure Drop

ΔT Temperature Difference

$\dot{m}$ Mass Flow Rate

$\dot{Q}$ Heat Transfer

$\dot{Q}_n$ Nominal Capacity

$\dot{Q}_r$ Additional Reserve Capacity

$\dot{Q}_{max}$ Maximum Capacity

$\dot{m}_{total}$ Total Mass Flux

λ Total Thermal Resistance [K/W]

μ_L Liquid Dynamic Viscosity

Φ_{fr} Two-Phase Friction Multiplier

ρ Fluid Density [kg/m^3]

ρ_G Density of the Vapor Phase

ρ_H Homogeneous Density

ρ_L Density of the Liquid Phase

σ Surface Tension of the Fluid

Θ The Angle of the Channel Relative to Horizontal

°C Celsius

c_p Specific Heat Capacity at Constant Pressure [J/(kg $\cdot K$)]

cm Centimeter

d Characteristic Length

f_L Liquid Friction Factor

Fr Froude Number

G Mass Velocity

g Gravitational Acceleration

H Height Difference

kW Kilowatt

l Liter

m Meter

mW Milliwatt

P Heat Load

p Pressure

R Thermal Resistance

$R_{conduction}$ Thermal Conduction Resistance [K/W]

$R_{convection}$ Thermal Convection Resistance [K/W]

R_{total} Total Thermal Resistance [K/W]

Re_L Reynolds Number for Liquid Flow

T Temperature

T_{amb} Ambient Temperature [$^{\circ}C$]

T_{ex} Temperature at the Gas Cooler Exit

V Volume

W Watt

We Weber Number

(v) Fluid Velocity [m/s]

2PACL 2-Phase Accumulator-Controlled Loop

$[EO]_n$ Ethylene Oxide

$[PO]_m$ Propylene Oxide

[R-OH] Alcohol

α Convective Heat Transfer Coefficient

η Dynamic Viscosity [Pa $\cdot s$]

λ Conductive Heat Transfer [W/(m $\cdot K$)]

f_{sub} Subcooling Correction Factors

$factor_{fp}$ Distributor Correction

Q_{requ} Heat Exchanger

Q_{selec} Cooling Capacity

δ Insulation Thickness [mm]

A Cross-Sectional Area

AMS02-Tracker Alpha Magnetic Spectrometer-02 Tracker

ATLAS AToroidal LHC ApparatuS

aTVS Active TVS

BSL Best Straight Line

CAD Computer-Aided Design

CMS Compact Muon Solenoid

CO_2 Carbon Dioxide

COP Coefficient of Performance

CU Condensing Unit

dp Pressure Differential

FS Full Scale

GWP Global Warming Potential

ISO International Organization for Standardization

ISS International Space Station

K Kelvin

kg Kilogram

kJ Kilojoule

LHC Large Hadron Collider

LHCb Large Hadron Collider beauty

m^3 Cubic Meter

mm Millimeter

MOP Maximum Operation Pressure or Motor Overload Protection

ND	Non-Detergent
Nu	Nusselt Number
P&ID	Piping and Instrumentation Diagram
PAG	Polyalkylene Glycol
ph	Pressure-Enthalpy
POE	Polyol Ester
Pr	Prandtl Number
pTVS	Passive Thermodynamic Venting
PVE	Polyvinyl Esther
PWR	Pressurized Water Reactor
Re	Reynolds Number
rpm	Revolutions per Minute
SC	Subcooling
SCADA	Supervisory Control and Data Acquisition
SH	Superheat
T_c	Condensing Temperature
T_e	Evaporating Temperature
TXV	Thermostatic Expansion Valve
x	Vapor Quality
λ	Thermal conductivity [W/mK]
σ	Standard Deviation

1 Introduction

CERN, the European Organization for Nuclear Research, is a world-leading research facility located in Geneva, Switzerland, where physicists and engineers study the base constitutions of matter. Funded by its member countries, CERN reciprocates the contributions through wages, goods and services.
A key instrument for high-energy physics research at CERN is the Large Hadron Collider (LHC), the largest and highest energy particle collider in the world. The LHC is part of the accelerator complex, shown in Figure 1. In the collider, situated 80 to 100 m underground, two particle beams are accelerated close to the speed of light and made to collide. A sequence of detectors is arranged concentrically around the interaction point, capturing the fundamental effects at work. The detectors form the core of the four experimental facilities distributed across the LHC, with ATLAS (A Toroidal LHC ApparatuS) and CMS (Compact Muon Solenoid) being the most notable. The detector is immersed in a uniform magnetic field so that the charged particles are directed onto a circular path by the Lorentz force.

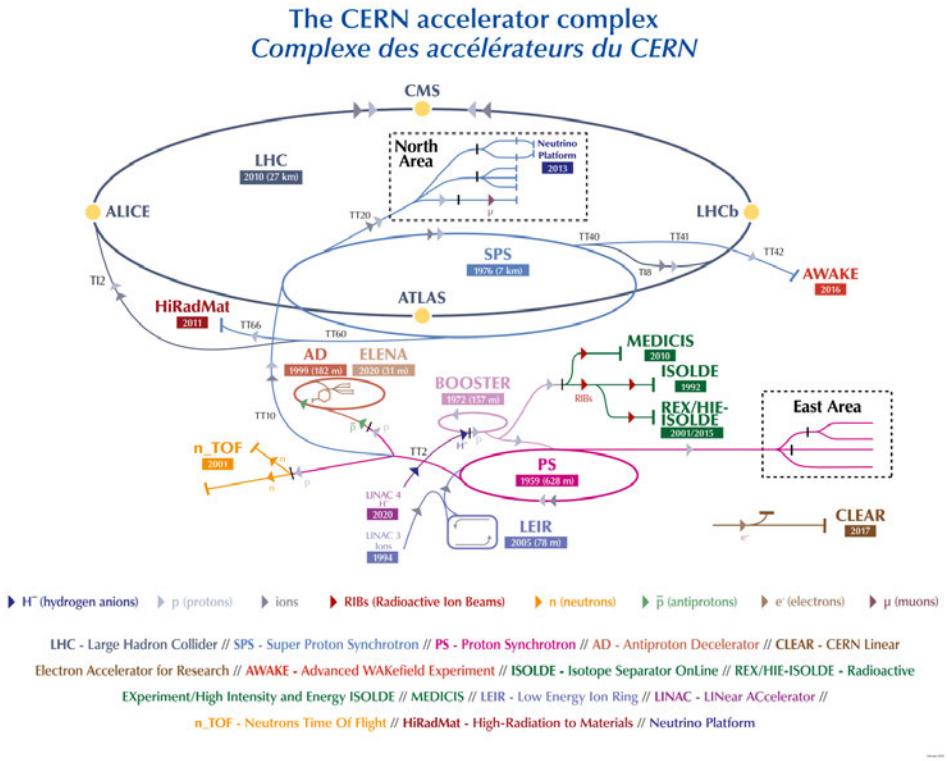

Figure 1: CERN accelerator complex (*The accelerator complex | CERN* 2025)

Briefly, the detectors are build up of three layers, that enable the identification of the particles resulting from the collision. The inner tracker detectors are the closest to the interaction point and composed of silicon-based semiconductors densely organized in planes, which interact with the charged particles and enable detection in space. To better identify the particle already tracked by the inner detector, the calorimeters measure its energy. Muons, electron like particles with a very low chance of interaction, pass undetected through the previous layers and their trajectory and energy are captured by the largest detectors, the muon spectrometers.

The two largest detectors, CMS and ATLAS will undergo a major upgrade in 2025, the Phase II Upgrade. Schmidt 2016 gives information about the key points of the upgrade program of the four major experiments and the physical background. A key point relevant for thermal management of detectors is the increased radiation. Especially for the detectors at smaller radii, which are more exposed to the radiation.

1.1 Detector Cooling

The cooling of particle detectors at CERN has evolved significantly since the 1960s, driven by the need for low-temperature technologies in high-energy physics experiments. Development in silicon detector technology imposes requirements for detector cooling, ensuring reliable performance over a lifetime of 10 years. The requirements, eager to be kept, can be summarized as follows:

- Thermal constraints
  - The dissipation of generated heat combined with the electronic power generated by the high-energy silicon chips is of significant importance for optimal operation.
  - Silicon is sensitive to large temperature fluctuations in the cold temperature range.
- Radiation protection
  - At smaller radii, the radiation intensity increases and thus the temperature must be lower, down to -30°C at the inner layer.
  - To protect the sensors from radiation damage caused by beam collisions, they are best kept well below 0°C.
- Reduced overall system mass to enhance physics results
  - For optimal data capturing, the particle's interaction with material in the detector must be kept at a minimum.
  - Optimized cooling system mass, such as a small refrigerant mass and a thin wall thickness of pipes.

Carbon dioxide (CO_2) has proved itself as a refrigerant for silicon detectors: excellent thermal properties, which enable small diameter tubes and resistance to radiation damage. These advancements aim to meet the challenges of maintaining sub-zero temperatures for silicon sensors while minimizing material budget and ensuring radiation resistance in high-luminosity environments, (Bart Verlaat and Colijn 2009).
Environmental-friendly cooling systems are replacing conventional refrigerants, like fluorocarbons in the ATLAS and CMS experiments, as these fluids have high global warming potentials (5000–10000*GWP_{CO_2}), as noted by Hallewell 2023. This is achieved by utilizing innovative transcritical R744 cycles for primary chillers in addition to the oil-free secondary CO_2 pumped loops (Zwalinski et al. 2023).

1.2 2PACL (2-Phase Accumulator-Controlled Loop)

Since oil-lubricated machinery is banned from fluid circulating systems in the detector area, the secondary CO_2 cooling plant is not a vapor compression cycle, but a pumped loop controlled by an accumulator. The 2PACL concept was developed at Nikhef in the Netherlands and was installed on the ISS (International Space Station) in 2011 to remove heat by evaporative cooling from the AMS02-Tracker (Alpha Magnetic Spectrometer-02 Tracker) silicon detector. The main components of the 2PACL system, as well as the operational schematic in the pressure-enthalpy (ph) diagram are displayed in Figure 2.

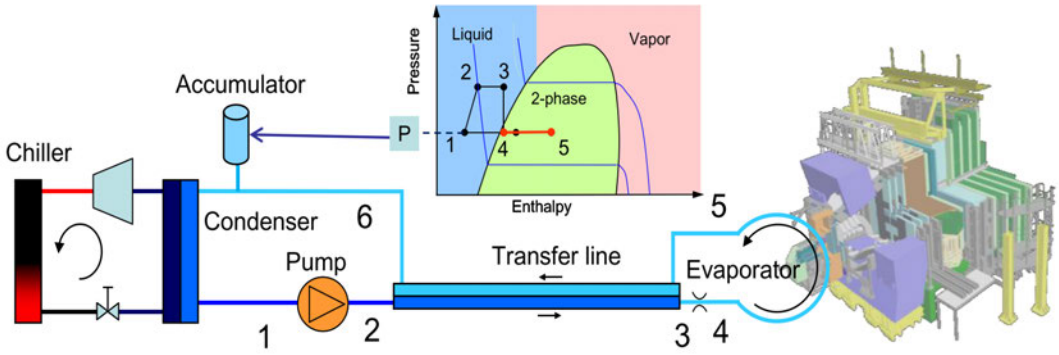

Figure 2: The 2PACL of LHCb-VTCS (Large Hadron Collider beauty Vertex Locator Thermal Control System) (Bart Verlaat and Colijn 2009)

The saturation temperature in the cooling system is controlled through pressure regulation by heating and cooling the liquid/vapor CO_2 pool in the accumulators. Each accumulator is equipped with an electrical heater and a heat exchanger powered by the primary system for cooling down the liquid. The 2PACL concept allows a minimal amount of hardware in the experimental cavern and most of the equipment in accessible areas, the service cavern. In case of active components failing, they can be exchanged or checked, protected from radiation and the magnetic field in the experimental cavern.
A concentric transfer line is connecting the plant to the evaporators in the detector. The high-pressure liquid is flowing on the inside while the 2-phase vapor is returning on the outside of the transfer line. Saturated liquid entering the distributing manifolds in the detector area enables a more stable flow distribution compared to vapor.
To prevent drying out into the superheated region, an overflow of liquid is sent to the detector. Thus, a vapor quality between 0% and up to 30-50% is maintained. This range of vapor quality also offers optimal heat transfer properties.
To serve all operational conditions, a 2PACL plant has an accumulator volume of about three times the system volume and has been successfully implemented in various experiments at CERN, including LHCb's Vertex Locator and CMS's pixel detector upgrade (Verlaat, Lysebetten, and Beuzekom 2008).

1.3 Phase II Upgrade

Since 2008, parts of 3 detectors at CERN are cooled with CO_2. For accurate temperature control under all operational conditions a pumped cycle was developed. The cooling capacities range from 1 to 15 kW at a evaporation temperature of -30°C. The requirements of the Phase II upgrade demand for cooling power of 300 to 550 kW at -45°C for roughly 1000 evaporators in parallel. Precautions must be taken, as the increased cooling capacity requires a larger system volume and a scaled-up primary cooling system. Due to the spacial restrictions underground, both the primary system and an additional CO_2 storage vessel will be located on the surface.

1.4 Surface Storage

The larger system volume requires larger high pressure accumulators, as the accumulator volume is three times system's. For 300-400 l system volume, a 1 m^3 accumulator is required, which is not feasible, due to spacial restrictions in the service cavern and the associated high cost. To operate the large cooling plant a substantial storage vessel must be implemented. Since the space is limited in the experimental cavern and to avoid a large amount of CO_2 stored underground, the sufficient integration capacity is held by a vessel located on the surface (Verlaat, Lysebetten, and Beuzekom 2008). This vessel is called surface storage and is shown in Figure 3. It includes a shed beneath the main structure, which houses technical components such as valves and piping for system integration and vessel filling operations.
The surface storage is kept at a constant pressure, controlled by electrical heating and cooling, provided by the primary cooling system. Meanwhile, a natural convective loop constantly circulates liquid between the vessel and the underground plant level, this is elaborated in Section 1.4.1. Figure 4 provides an overview of how the vessel is integrated into the 2PACL system and displays the directions of flow.
As a result of dynamic operations, such as changes in cooling power or pressure setpoint, the vessel can be filled with or drained of CO_2 reacting to certain accumulator liquid-level thresholds. As the accumulator is the main pressure control object, the surface storage operates only when the accumulator liquid level exceeds its minimum or maximum thresholds, as a continuous operation would lead to instabilities. Under stable conditions, surface storage control is not required and the temperature stability on the detector side is maintained – one of the key benefits of the 2PACL system (Bart Verlaat, Petagna, et al. 2019).
When fluid is received by the surface storage vessel, vapor is condensed at the heat exchangers on top of the vessel to counteract pressurization. Once fluid is drained, electrical heaters evaporate liquid to pressurize the storage volume. To ensure that CO_2 can always be released from the plant to the surface, the surface storage pressure, including the static head pressure due to gravity, must always be at a lower value than the pump discharge, the high-pressure side of the plant. Vice versa, keeping the pump inlet, the low-pressure side, always lower in pressure than the surface storage allows the replenishing of fluid to the plant (Verlaat 2023).

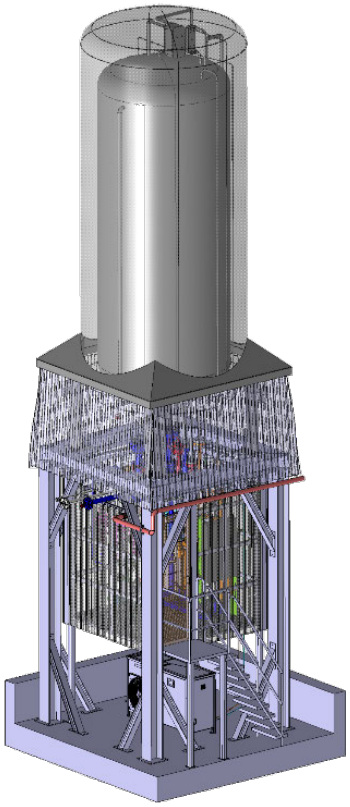

Figure 3: CAD (Computer-Aided Design) model of the surface storage, including the beneath shed.

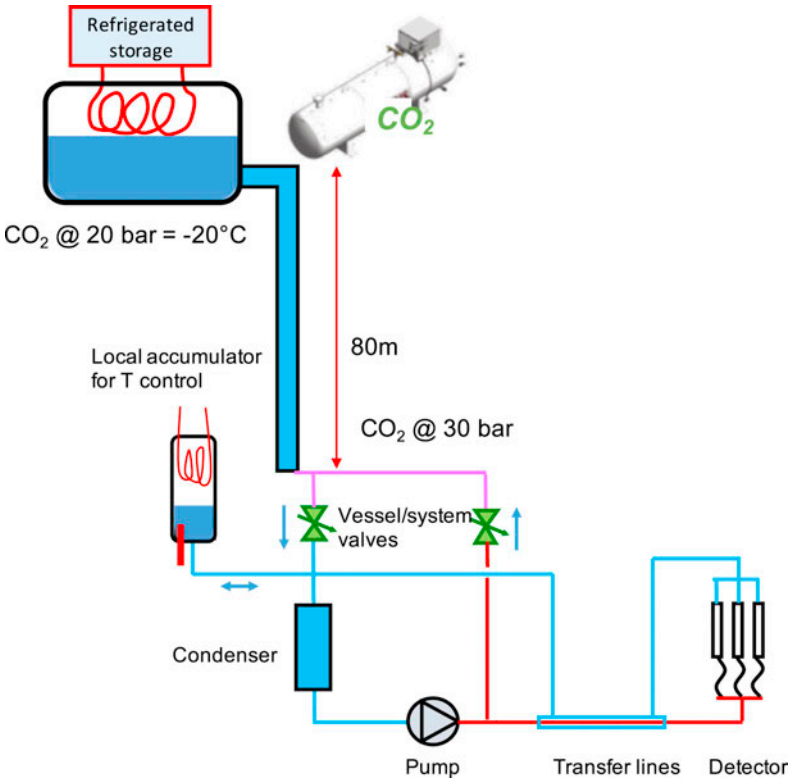

Figure 4: CO_2 plant regulation and storage system schematic (Tropea et al. 2019).

1.4.1 Thermosiphon Loop

Natural circulation loops transport heat from a source to a sink without fluid displacement machines, such as pumps. Since the pressure difference, creating the motive force for flow is not induced by moving parts, the cycle is less prone to failure and maintenance. The loop consists of a heat source and a heat sink, interconnected by piping. The configuration illustrated in Figure 5 highlights the continuous circulation path. Given the source and sink conditions are constant and the integrity of the closed loop is maintained, the circulation can continue indefinitely. The circulation is driven by buoyancy forces caused by density differences under the influence of a gravity field. As the heat source transfers thermal energy to the fluid, its density decreases and it rises. Then, after rejecting the heat to the sink, the density is again increased and thereby the convective flow is sustained (Vijayan and Nayak 2005).

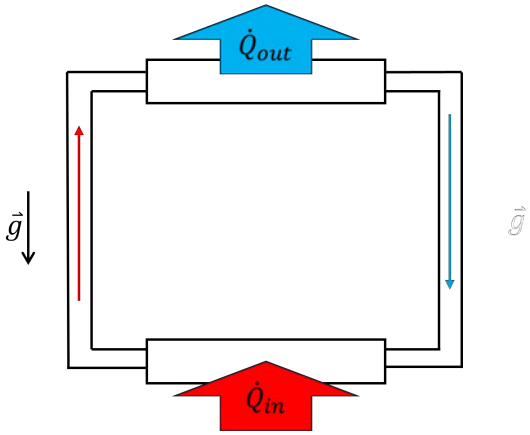

Figure 5: Thermosiphon loop, natural circulation scheme under influence of gravity.

The flow's magnitude in the loop is defined by the pressure differential over the heat sink, which is caused by the height and density differences of the loop's hot and cold legs. The equation for the static height pressure, containing the density (ρ), gravitational acceleration (g) and the height difference (H), is:

$$p = \rho g H \tag{1}$$

This equation shows the dependency: as the density is the only variable that changes from sink inlet to outlet, it is the driving force.

1.4.2 Thermosiphon Loop in the Surface Storage

A natural circulation system is established between the liquid feed pipe and the return pipe, according to the thermosiphon principle. The purpose is to bring subcooled liquid to the plant underground and return vapor from the plant by convection without using a pump, for simplicity. The integration of the surface storage and a schematic representation of the piping is given in Figure 6.

The pipe for the liquid outlet is positioned at the bottom of the vessel, extracting the liquid of highest density. A non-return valve is installed to ensure that flow can exit only. Returning flow is entering the vessel from the bottom, but its pipe extends $50\ cm$ into the vessel, so the incoming flow is less likely to mix with the outlet.

To initiate the convective flow the EH6062 start-up heaters are located underground in the return line slope. Once the heater generated sufficient vapor and thus set the convective flow in motion, the heater can be switched off. The vapor returning from the detector and the heat transfer due to the ambient heat leak in the return pipe perpetuate the continuous convective flow.

The thermosiphon effect is further optimized by sloped pipe sections ($> 1\ cm/m$) instead of horizontal, enhancing convective flow. Additionally, a spiral heat exchanger ($5\ kW$) is installed

on the liquid feed pipe before the line descends into the cavern to supply the plants, sub-cooling the liquid exiting the storage vessel. This sub-cooling further amplifies the thermosiphon effect, ensuring an efficient and self-sustaining convective cycle.

Replenishing of the plants is realized by merging of the flow from the feed pipe with the 2-phase liquid returning from the detector. The flow is directed to the sub-cooler inlet upstream of the pump. For the draining of the plant the return line extracts vapor from the heat exchanger inlets of the accumulators. A second method of filling the storage vessel involves the supply line: between the HX6006 and the non-return valve the flow can be redirected to an intersecting pipe ascending along the vessel's wall. A spray nozzle, positioned high on the vessel's vertical wall, spraying the subcooled liquid into the vapor phase. This approach facilitates not only the filling of the vessel but also aiding in the recondensation process, helping to counteract the resulting rise in pressure.

For the thermosiphon loop, a second pipe dedicated for returning flow only is not necessarily needed but ensures that no vapor counter flow occurs. This vapor could get caught up in siphon-like structures created by faulty installation of pipes.

In the event of primary system fail, the loop is already running and the heat leak will keep it running to an extend, causing fluid motion inside the vessel.

1.5 Pressure Regulation and Safety Cooling System

The surface storage vessel is designed to operate within a specific pressure range, which must be maintained at all times. During standard operation, the primary system is providing cooling according to surface storage setpoints, whereas always maintaining a pressure well below the design pressure threshold.
In the event of a primary cooling system failure, an emergency system (Figure 6, "Back-up chiller") must overtake to prevent over-pressurization, which could otherwise result in refrigerant loss due to venting through safety valves. However, this emergency cooling system is not intended to replace the primary system's functionality. Instead, its role is to intercept the heat leak and thus maintaining system integrity until the primary cooling system is restored.

1.6 Problem Statement

Despite the critical role of the emergency cooling system, its design is inherently limited to temporary intervention. A heat leak quantification under failure conditions will give information about the magnitude of the required cooling capacity of the back-up system. The system's reliability to effectively respond to a primary cooling failure is essential to prevent refrigerant loss through safety valves and a safe operation until the primary system is re-established is a central safety concern.
The concept of a suitable design, while weighing off available options is subject of this thesis.

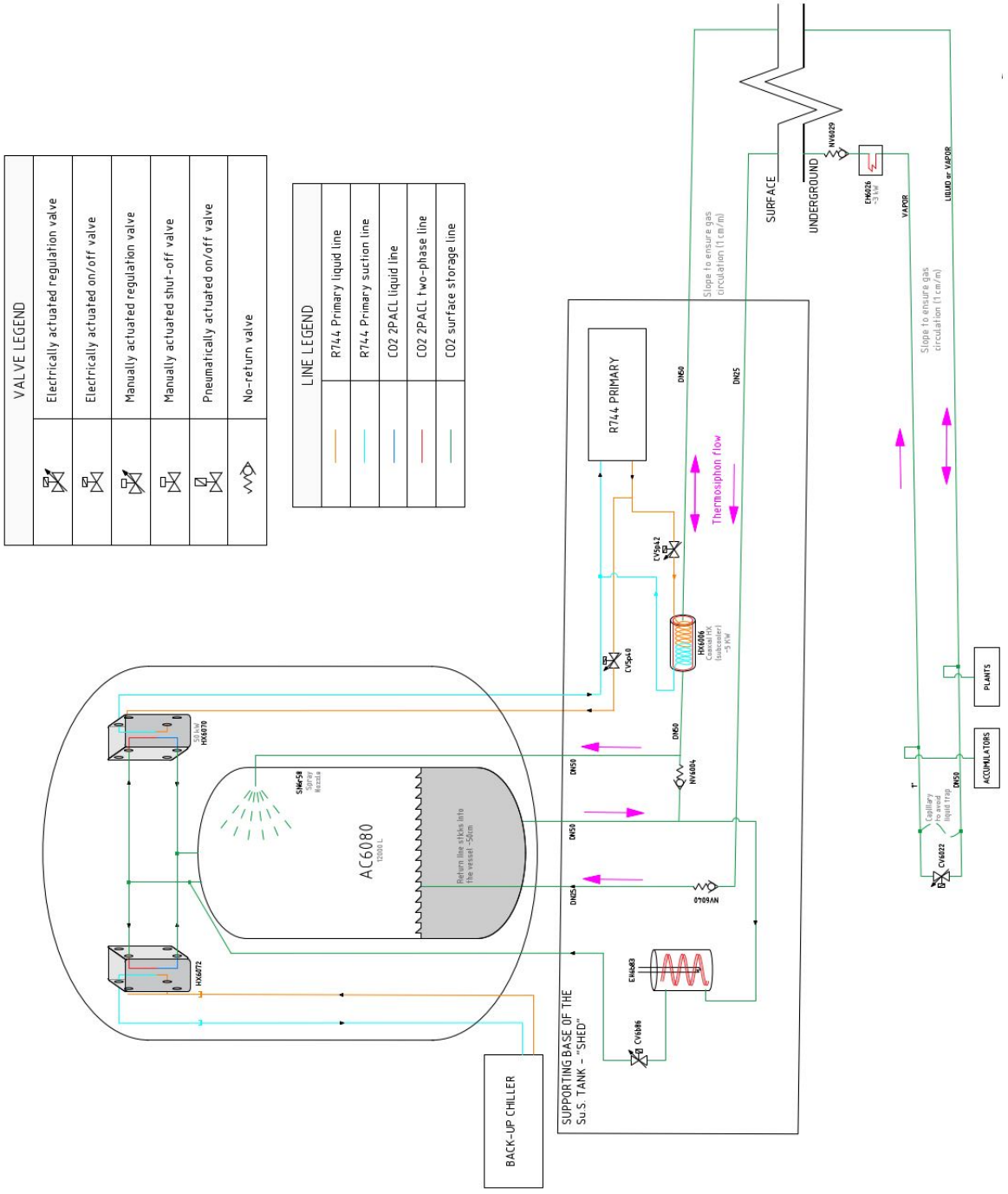

Figure 6: Simplified P&ID (Piping and Instrumentation Diagram) of the surface storage and the thermosiphon loop.

2 Theoretical Framework

This chapter provides a literature review on pressure regulation solutions, present on the market. Furthermore, researched methods and comparable solutions relevant to the topic are elaborated.
The chapter further examines subjects related to the vapor compression cycle and the influence of a height difference between condensing unit and evaporator, as this approach is a promising candidate for the emergency cooling system.
Moreover, the heat leak evaluation is detailed and the calculation of the pressurization rate in reference to the literature. The chapter is rounded up by an analysis of pressure drop of moving fluids in pipes along with an explanation of two selected correlations for single and two phase flow relevant for this work.

2.1 Pressure Regulation in Cryogenic Vessels

Vessels designed for fluid storage are equipped with a pressure regulation system to prevent over-pressurization due to over-filling or thermal expansion. Vice versa, a collapse of the tank induced by pressure reduction must also be compensated, initiated by draining fluid from the tank. To mitigate the risk of structural failure and associated consequences, a pressure management system is mandatory.
The surface storage is equipped with a heat exchanger on top of the vessel, cooled by the primary system for pressure regulation, intercepting to the heat leak and matching of setpoints during active operation. Thermal insulation as a passive precaution, and active precautions, used or researched in storage vessels or tank-like systems, are briefly explained here. The eligibility of findings will be evaluated for the Surface Storage project to assess their relevance in this specific application of a safety cooling system.

2.1.1 Insulation and Vessel Material

Insulation and tank material influence the heat transfer between the stored fluid and the ambient conditions. Pressurized vessels for stationary use are most commonly made of steel due to its durability and strength. The surface storage vessel's service pressure is 45 bar, which is a common value for cryogenic tanks. Increasing the design pressure beyond this limit would require significant modifications, including different materials and wall thickness to reach higher pressures. Developing a custom tank, specified for pressure ratings beyond 45 bar would result in substantial costs, making it less economically feasible compared to commercially available vessels.
A common, inexpensive and effective insulation method is evacuated perlite, which is also used for the surface storage's insulation. In this approach, the enclosed volume of the double-wall structure is filled with perlite powder and is evacuated to minimize heat transfer. Perlite is a volcanic rock, which is crushed and heated to vaporize the contained water, causing the material to expand. The porous granules get sieved into various grades depending on desired insulation properties.

2.1.2 Pressure Regulation in Storage Vessels

Manufacturers of cryogenic and medium-pressure vessels equip their systems with pressure relief valves to maintain a pressure while sacrificing fluid and companies like AG n.d. provide a boil-off rate in $\%_{Volume}$ per day.
Options for pressure increase are heaters or gas inlets. Tank blanketing valves, like from Inc. n.d., induce inert gas into the blanket layer of gas into the vessel to prevent vacuum formation while fluid is drained. This feature, however, is used for low-pressure applications. Additionally, the company suggests the intake of ambient air is considered a method to maintain pressure stability during draining scenarios in Inc. 2017. This source further presents a vent of a larger diameter to prevent catastrophic events, a common feature in pressurized tanks.

2.1.3 Reduction of Boil-off Losses in Propellant Tanks

On behalf of NASA, Lin, Vandresar, and Hasan 1991 were investigating the self-pressurization of a liquid hydrogen cryogenic vessel due to heat leak through thermal protection systems during space experiments. In their paper, pressure control methods, shown in Figure 7, such as mixing, passive thermodynamic venting (pTVS), and active TVS (aTVS) were investigated theoretically.

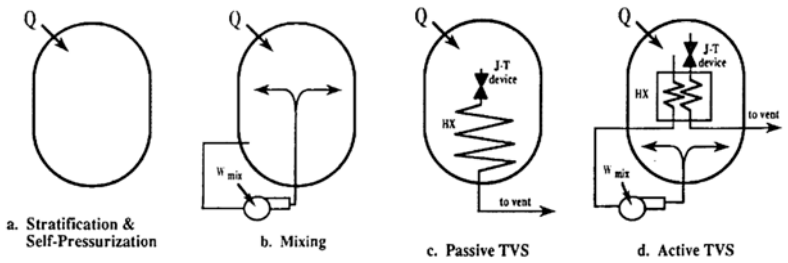

Figure 7: Schematic representation of self-pressurization and pressure control technologies by Lin, Vandresar, and Hasan 1991

The heat flux across the vessel's walls leads to thermal stratification, the layer formation of varying density in a gravity field. Mixing of these layers and thus unifying the temperature of the fluid inside the vessel is decreasing the pressure of the vapor phase acting on the walls, as the vapor layer is the layer with the highest temperature and pressure. Destroying the arrangement of distinct layers by directing liquid from the bottom layer and spraying it into the vapor phase is stimulating interfacial heat transfer and results in a pressure reduction. However, mixing would be effective for short-term use only, in both fuel tanks on space missions and stationary storage vessels.
The method of pTVS involves a Joule-Thomson device and a heat exchanger within the tank, as shown in Figure 7 (c.). Since an expansion can only be realized from a region of high pressure into a lower pressure environment, this method involves venting of the stored fluid. The high pressure liquid gets expanded and flushes through a heat exchanger, extracting heat from the stored fluid. Utilizing the temperature drop associated with the expansion for cooling purposes, minimizes the amount of fluid during venting and thereby increases the efficiency of

the pressure reduction process. Increasing the effectiveness of a venting process aligns with the primary function of a storage tank. Nevertheless, venting itself is to be considered for the intended application as it involves fluid loss or release. Additionally, researchers suspect a long response time of attempted pressure control.
The combination of both, thermodynamic venting and mixing is aTVS (d.). The gas from the expansion is now directed to cool the pump inlet of the mixing device. Subcooled liquid is sprayed into the vapor phase and enhances the efficiency of the mixing method, while throttled fluid gets released from the tank.
Solutions to eliminate the boil-off losses, the release of fluid, to maintain a design pressure, was examined by Christie et al. 2011. An active technique, a dedicated multistage cryogenic cycle should cool the shell of the fuel tank of spacecrafts (”Broad area cooling”) combined with an multilayer insulation as the passive technique. However, the requirements of space experiments differ significantly from the pressure regulation of a CO_2 storage vessel on earth, as the cryo coolers are providing 6 to 80 W cooling capacity at 90 °K. The surface storage's heat leak, including the thermosiphon, will be calculated in a following chapter, but is very likely to be several orders of magnitude higher with the provided cooling in the range of -10 to 10 degrees.

2.1.4 Pressurizers in Nuclear Power Plants

In pressurized water reactor (PWR) nuclear power plants (Figure 8), a pressurizer maintains a pressure in the closed liquid system, that is subject to temperature and liquid volume changes, for a controlled cooling of the reactor Honert 1969. The pressurizer vessel is equipped with electrical heaters for pressure increase and counteract heat losses and a spray nozzle to inject subcooled water into the vapor phase and thus reducing pressure inside the tank.

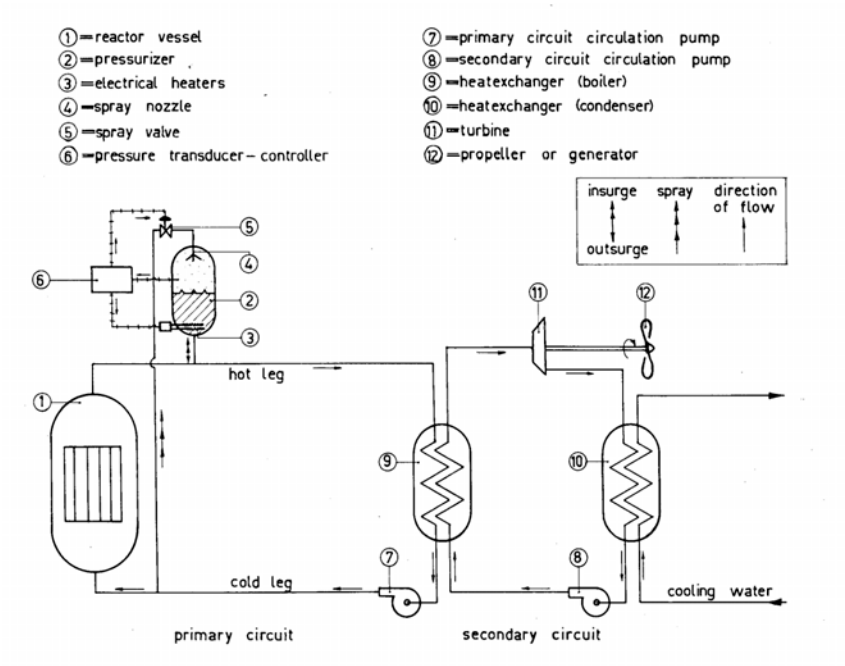

Figure 8: Schematic layout of a PWR power plant

The pressurizer is an active component in the cooling loop and allows for dynamic operations of a nuclear reactor, like power transients in ship propulsion plants.

2.1.5 Conclusions

The heat leak of the surface storage is not only due to the insulation of the vessel itself, but also a larger proportion is contributed by the thermosiphon piping. The magnitude of the overall heat leak is evaluated in a later chapter. However, the heat pick-up must be intercepted, in order to maintain the design pressure of the vessel of 45 bar. It is interesting to note, that the presented mixing strategy is to an extent also present in the surface storage. The natural convection due to the thermosiphon piping's heat leak is likely to cause a swirl inside the vessel and thereby destroying layer formations.
Methods for pressure regulation in pressurized vessels have been elaborated. As the surface storage is an extension of the system volume, periodic venting is not an option, which would be a commonly used method. Even though, compared to other refrigerants, CO_2 is not as climate damaging, one of the leading approaches for the 2PACL system is the environmental friendliness, which would be compromised. Furthermore, releasing refrigerant on a regular basis is inconvenient and cost-intensive. Concluding is to say, that the options presented by manufacturer companies are not eligible to the surface storage pressure regulation approach.
Apart from the venting as a pressure regulation method, NASA has investigated a broad area cooling within the double shell of a vessel. Tests conducted by Plachta, Johnson, and Feller 2015 proved it to be a sufficient method to achieve zero boil-off.
However, in the surface storage system, the primary cooling system already reduces temperature by operating a heat exchanger on top of the vessel through natural convection. Therefore, a second heat exchanger also operated by a dedicated vapor compression cycle is a convenient, redundant, and straightforward solution to intercept the heat leak and consequently maintain design pressure.
This setup results in a three-level pressure regulation system:

I. Primary cooling system (vapor compression cycle)
II. Emergency cooling system (redundant vapor compression cycle)
III. Venting as a last resort for pressure relief

This approach ensures system reliability by adding a level of redundancy in case of primary chiller failure, minimizing CO_2 venting to maintain service pressure.

2.2 Vapor Compression Cycle

The cycle constitutes of four processes: compression, heat rejection, expansion, heat absorption. While compression and heat rejection are commonly done in compact condensing units, which is elaborated in Chapter 3, the components for expansion and heat absorption demand for separate consideration.

2.2.1 Expansion Devices

A throttling device allows the refrigerant to expand from the high pressure after the gas cooler to the low evaporating pressure, undergoing an isenthalpic process. Expansion devices can be divided into the categories of fixed or variable cross-section, where the opening of the orifice can be electrically or mechanically controlled. Since a redundant system is required, additional controls are not acceptable; thus, only mechanical solutions are part of this work.

Capillary Tube A capillary tube is a type of fixed orifice throttling device, consisting of a narrow pipe of uniform diameter across its length. It is a simple and cost-effective component, commonly used in smaller or steady-load systems where precise control is less critical.
Every fixed orifice throttling device must be dimensioned carefully as it cannot flexibly adjust to load changes or operational instabilities. Dependent on the upstream pressure regulation, a bypass might be needed to avoid excessive pressure increase due to the flow resistance of the throttling device (Sunu et al. 2018).

Thermostatic Expansion Valve (TXV) The thermostatic expansion device, a type of variable orifice throttling device, is actively throttling the mass flow according to the evaporator outlet temperature, metering flow at a rate equal to the evaporation.
The thermostatic expansion valve consists of the valve body, orifice, sensing bulb and its capillary, adjustable spring, diaphragm and pressure equalization port (Figure 9).
As the TXV is metering refrigerant to the evaporator, its maximum capacity can be translated to maximum mass flow and is determined by the orifice and the valve's body. Thus, orifice and body must be chosen according to the system requirements.

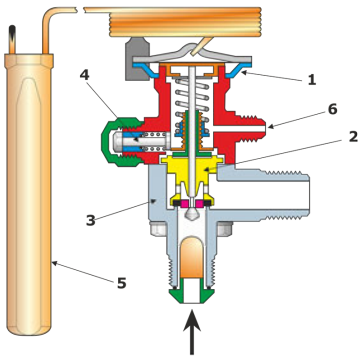

Figure 9: A thermostatic expansion valve. (1) Membrane housing, (2) Interchangeable adapter, (3) Valve housing, (4) Spindle for adjusting static superheat, (5) Refrigerant-filled bulb, (6) Port for external equalization. (*4.2 Thermal expansion valves (TEVs) - SWEP* 2025)

As a result to a force equilibrium across the diaphragm, shown in Figure 10, the valve opens or closes. Three pressures are extorted on the TXV's membrane:

1. The TXV bulb pressure, a converted temperature, sensed on the evaporator exit.
2. The equalization line, transmitted evaporator saturation pressure.
3. Spring pressure, an adjustable tension.

The sum of 2. and 3. against 1. in equilibrium determines the opening of the valve.

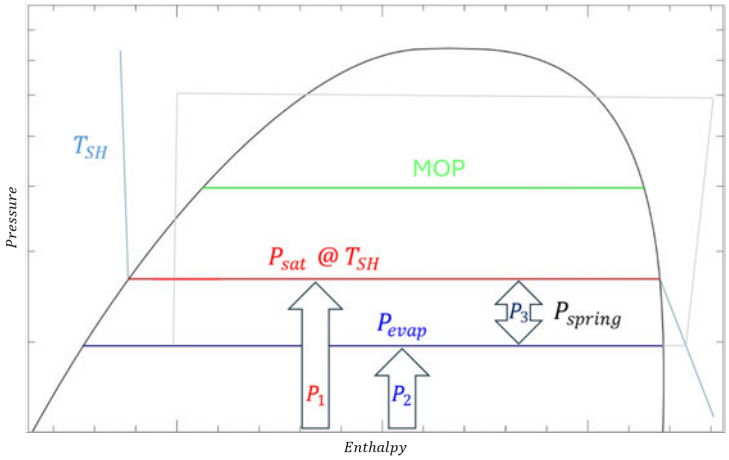

Figure 10: Pressure equilibrium across diaphragm and maximum operation pressure (MOP) of thermostatic expansion valve displayed in logp-h diagram.

The sensing bulb is filled with refrigerant, that is in saturated state during operational conditions. Mounted to the exit line of the evaporator, it is sensing the temperature and the saturation pressure of the bulb's filling establishes. This sensing happens with an inevitable delay due to thermal inertia of the bulb and the heat transfer resistance between the flow inside the tube and the medium inside the bulb. As noted by Eames, Milazzo, and Maidment 2014, the bulb charges, considerable for TXVs are straight-charge or cross-charge. The straight-charged bulbs are filled with the same refrigerant used in the cooling loop, whereas the cross-charged is filled with a different refrigerant or a blend.
Facing the saturation pressure at the sensed temperature, is the saturation pressure at the evaporating temperature. The equalization port connects the bottom side of the diaphragm with the evaporator outlet and transmits a closing force to the valve. However, the comparison of these pressures will result in a valve opening tendency within the design range of the TXV.

The force applied by the spring to the diaphragm is supporting the equalization pressure, resulting in a closing tendency. As the pretension to the spring is adjustable, the temperature on the evaporator outlet, responsible for the valve to open, can be tuned.

The MOP (Maximum Operation Pressure or Motor Overload Protection), as shown in Figure 10, is a feature of cross-charged bulbs. The chosen filling ensures the liquid proportion to be evaporated above a specified evaporator outlet pressure and the associated evaporation pressure inside the bulb. The valve will close gradually until it is fully shut, to protect the components in

the cooling loop from overpressure, (Danfoss 2005). MOP charges with ballast have an additional thermal mass integrated in the bulb, enhancing latency of the TXV system. This is useful to control the superheat of evaporators with dynamic load changes.

A superheat between 5 K and 10 K is advised, since it protects the the compressor from sucking liquid and ensures a sufficient utilization of the evaporator (Eames, Milazzo, and Maidment 2014). The evaporator utilization is an important proportion to the overall efficiency, as the heat transfer due to evaporation is more efficient than by superheating vapor. Efficient evaporation allows for greater heat removal at the same mass flow rate. In Figure 11, the composition of superheat is shown. The operating superheat consists of two proportions: the static superheat, which sets a minimum amount of superheat, usually between 3-4 K, and once the valve opens, an opening superheat not higher than additional 5 K is advised, as noted by the same authors.

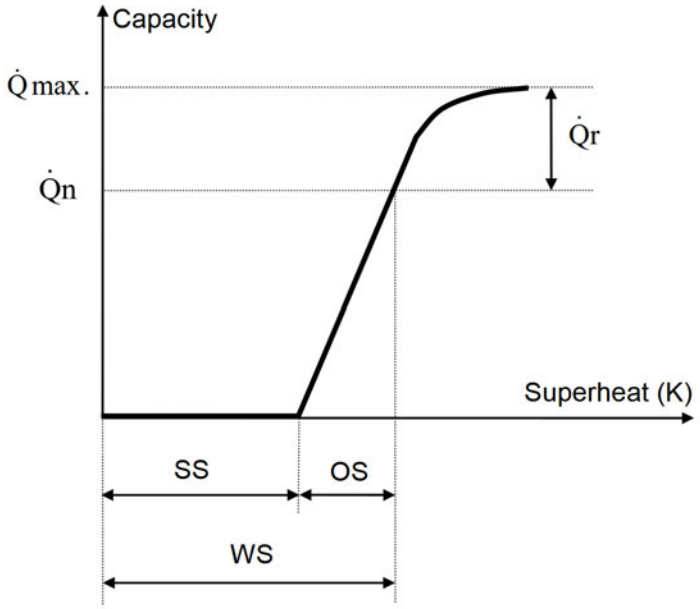

Figure 11: Range of Capacity and Superheat (*Statements: Capacity Rating of Expansion Valves - ASERCOM* n.d.)

The plot also states that the nominal capacity ($\dot{Q}_n$) can be exceeded by an additional reserve capacity ($\dot{Q}_r$), allowing for more refrigerant flow. By adjusting the tension of the adjustment screw the force applied by the spring is modified, and thereby influencing the static superheat. A looser reduces the closing force and effectively shifts the graph to the left, reducing the static superheat. Conversely, a stiffer spring increases the closing force and result in a higher static superheat and increased working superheat across the capacity range as a result. However, the maximum capacity ($\dot{Q}_{max}$) is depending on the valve body's size and comes with the highest superheat. Excessive superheat and thus an elevated compressor inlet temperature results in significantly higher discharge temperature at the same pressure ratio. Exceeding the safe operational limits of the compressor compromises its efficiency and longevity. Furthermore, the higher temperature of the discharge gas may exceed the operational design considerations of the gas cooler. This leads to difficulties in the heat rejection and will cause a higher gas

cooler outlet temperature, ultimately leading to high vapor qualities after expansion from the high-pressure side. Consequently, this affects the phase distribution in the receiver and downstream components, influencing overall system efficiency and stability.

2.2.2 Evaporator

Already specified in the design of the surface storage is the heat exchanger for the primary system on top of the vessel, a 50 kW brazed plate heat exchanger featuring 84 plates. The supplier is a company known to the department that has proven itself, SWEP.
The Brazed Plate Heat Exchanger is constructed as a plate package of grooved channel plates with a filler material between each plate. During the vacuum brazing process, the filler material forms a brazed joint at every contact point between the plates, creating complex channels. This concept eliminates the necessity of gaskets and frame components, resulting in a compact heat exchanger.
The model, intended for the backup cooling system, its size and specifications are elaborated in this paper subsequent to the heat leak evaluation (Section 3.2).

2.2.3 Oil Management

Compressors, unless they are oil-free compressors, rely on sufficient lubrication. The oil management in refrigeration cycles is crucial, as lubrication of rotating parts reduces wear and maintain optimal performance.
Inside the crankcase of the compressor, a certain level of oil is maintained, which, during operation, mixes with the refrigerant and to an extent, ends up in the discharge of the compressor. Tang, Huang, and T. Li 2024 investigated the oil circulation rate in a vapor compression cycle and found dependencies to compressor speed, refrigerant charge, heat load and expansion valve opening. Many compressors feature a sight glass on the crankcase, to monitor the oil level. Often, an oil separator is installed downstream of the compressor to collect and return most of the oil from the discharge line. However, a small proportion of oil inevitably escapes and gets carried over to the downstream components, with a fraction eventually returning to the compressor crankcase. Over time, residual oil will accumulate in the downstream components, forming deposits. Horizontal pipes or local sinks are likely areas for oil collection. Insufficient oil entrainment back to the compressor can lead to inadequate lubrication, resulting in severe wear of bearings and contact surface of rotating parts and potentially fatal damage to the compressor. From an efficiency standpoint, the power required to overcome frictional drag is unavailable as useful power to the machine, reducing the compressor's overall performance. Additionally, oil film formation inside the evaporator, reducing the heat transfer efficiency, as it acts as a thermal barrier, as proven by Yoshioka, Kim, and Kasai 2008 for a CO_2 refrigeration system and PAG (Polyalkylene Glycol) oil as lubricant. Proper oil management is therefore essential for reliable operation and optimal performance.

CO_2 Systems Due to the outstanding solvency of CO_2, its acidic nature and ability to dissolve materials and fluids, it can degrade lubricants, an effect further amplified in the presence of moisture and high operational pressure. Therefore, the lubricant has to be chosen accordingly. Even during conventional subcritical operation, certain lubricants can be diluted excessively, leading to compromised lubrication of the system. This may result in issues, such as high oil carry-over, foaming and significant reduction of the efficiency, reliability or even severe damage to the compressor. In transcritical operation both temperatures and pressures are significantly elevated in respect to conventional operation, with pressures reaching more than three times higher. Therefore, selecting the appropriate lubricant for CO_2 refrigeration applications is of paramount importance (H. Li et al. 2002).

Karnaz 2022 provide insights on lubrication in CO_2 refrigeration and air conditioning applications. Three different types of lubricant types are predominantly used: Polyol Ester (POE), Polyalkylene Glycol (PAG) and Polyvinyl Esther (PVE). The chemistry of either one is manipulated to serve a specific purpose, so can the viscosity or miscibility and solubility with refrigerants vary within one kind.

2.3 Height Difference between Evaporator and Condensing Unit

The evaporator, cooling down the surface storage vessel, is located on the top of the vessel, at a height of 9 m above ground.

2.3.1 Performance

Considering a height difference in a vertical flow, the combined effect of static height pressure drop and frictional pressure drop must be accounted for. Thus, the provided pressure at the outlet of a chiller system, which is located significantly lower in respect to the evaporator, will not be maintained across the height difference. Assuming the expansion valve is located close to the evaporator, the loss in pressure downstream of the expansion device causes a loss in subcooling or even premature evaporation before refrigerant reaches the expansion valve.
Considering that the expansion device is located somewhere between the chiller and the evaporator, in addition to the pressure drop and associated downsides, the cooling capacity available at the evaporator may be reduced due to heat leak. The increase in enthalpy of the two-phase liquid also results in a rise in vapor quality, which has an effect on the flow regime and the heat transfer characteristics. This was investigated for vertical upstream CO_2 by Schmid et al. 2022.

2.3.2 Oil Entrainment

In the event of a height difference between chiller unit and evaporator, precautions must be followed more strictly to ensure proper oil transport throughout the whole setup. Oil accumulation can be prevented by carefully installing and supporting horizontal pipe sections and ensuring large bending radii. The pipe diameter must be sized to accommodate sufficient speed for the oil entrainment and optimal cooling performance, especially in the rising (up-flow) sections.

2.4 Calculation of Heat Leak and Pressurization

This section describes the heat leak calculation approach applied in this work. Subsequently, the method for an estimation of the pressurization rate is elaborated compared with findings from the literature.

2.4.1 Introduction of Heat Leak Calculations

The heat leak, the emergency cooling system must intercept, is calculated using Fourier's law (2). A temperature difference ΔT causes transfer of heat. The resistance against this flow is the thermal resistance R.

$$\dot{Q} = \frac{\Delta T}{R_{total}} = \frac{T_{amb} - T_{fluid}}{\Sigma R} \tag{2}$$

The thermal resistances of matter, such as the pipe and insulation, that limit the heat transfer from ambient to the fluid are:

$$R_{conduction} = \frac{\ln\left(\frac{d_{outer}}{d_{inner}}\right)}{2\pi\lambda L} \tag{3}$$

And with the conductance due to present (limiting) convection conditions inside, from the CO_2 flow and outside from natural convection.

$$R_{convection} = \frac{1}{\alpha\pi d L} \tag{4}$$

Relevant to the surface storage vessel and the thermosiphon loop's heat leak, is the **Convective Heat Transfer Coefficient (α)** represents the rate of convective heat transfer, in relation to an area [W m^{-2}]. It is mentioned in the definition of the Nusselt number (Nu), a dimensionless number that describes the ratio of convective to conductive heat transfer. The parameter d is the characteristic length, which, for flow in pipes, corresponds to the diameter, while the conductive heat transfer is represented by λ, the thermal conductivity of the pipe material, in relation to its thickness [W m^{-1}].

$$Nu = \frac{\alpha d}{\lambda} \tag{5}$$

The Dittus-Boelter Equation is a formulation for turbulent flow, which allows to calculate the Nusselt number. Since Reynolds numbers greater than 4000 are presumed turbulent and the values will be above this threshold, the following correlation is applicable in order to find the Nusselt number.

$$Nu = 0.023 Re^{0.8} Pr^{0.3} \tag{6}$$

In order to determine the Nusselt number, the Reynolds number and the Prandtl number have to be calculated.

The **Prandtl Number (Pr)** compares the relative size of the hydrodynamic boundary layer and that of the thermal boundary layer and hence, their relative importance in a flow. It does so by taking the ratio of momentum diffusivity (dynamic viscosity η) to thermal diffusivity, represented by the specific heat capacity over thermal conductivity of the fluid ($\lambda\, c_p^{-1}$).

A Prantdl number >1, as expected for CO_2, as it is $Pr = f(T, p)$, in the thermosiphon loop scenario, points out how the diffusivity of momentum is the dominating transport mechanic.

$$Pr = \frac{\eta c_p}{\lambda} \tag{7}$$

The **Reynolds Number (**Re**)** is a dimensionless number and used to determine a flow's regime. Laminar flow is assigned to $Re < 2000$, while Reynolds numbers greater than 4000 are considered turbulent. When $2000 < Re < 4000$ a flow is in a transitional state, where it is very unstable and strongly affected by time-dependent fluctuations. The Reynolds number represents the ratio of inertial forces, characterized by density (ρ and velocity (v), to the viscous forces resisting the flow, defined by the dynamic viscosity, η.

$$Re = \frac{\rho v d}{\eta} \tag{8}$$

2.4.2 Pressurization of the Surface Storage Vessel

Inside the vessel, pressure increases due to evaporation of liquid CO_2, caused by the heat leak. The primary heat pick-up comes from the CO_2 in the thermosiphon loop, and with a smaller contribution through the vessel's double shell, as the heat leak evaluation shows. As the temperature inside the system increases, the heat flux will decrease due to the lower temperature gradient to the outside.

Predicting the time of pressurization using a homogeneous model, that assumes a uniform temperature distribution within the tank, has been shown to deviate significantly from real conditions. As noted by Lin, Vandresar, and Hasan 1991, the homogeneous model gives a good baseline, as it is the slowest possible pressure rise rate, but under real conditions the rate is one to ten times faster. This observation is based on the unevenly distributed energy along the vertical axis of the tank, that Z. Li et al. 2023 elaborated. The density-driven stratification results in a distinct layer formation, with the uppermost layer dictating the critical pressure present inside the vessel.

However, the heat leak of the surface storage vessel, that mainly comes from the thermosiphon's piping will induce a fluid motion by extracting liquid from the bottom and returning fluid. This may lead to a more uniform temperature distribution, than in conventional storage vessels, where the fluid remains stagnant, allowing buoyancy-driven stratification to develop unhindered.

Assuming the vessel and thermosiphon piping are filled with saturated liquid and a proportion of saturated vapor, the filling level can be associated with the vapor quality. As the pressurization is an isochoric process, the change in enthalpy can be taken from the path of constant density connecting the initial vapor quality and the upper pressure threshold.

Time of Pressurization For the calculation of the time of pressurization, the vessel is assumed to contain saturated liquid and a proportion of saturated vapor and thus, a uniform temperature distribution. The density is calculated by:

$$\rho_{filling} = \frac{m_{filling}}{(V_{vessel} + V_{thermosiphon})} \tag{9}$$

Since the pressurization is an isochoric process, between the setpoint temperature and the upper pressure threshold the enthalpy difference is calculated using the same density. The heat leak decreases, as the temperature inside the vessel rises, but is simplified to a constant value here. The value is interpolated between the setpoint temperature and the temperature corresponding to the upper threshold, using the linear trend created in the heat leak evaluation section (Section 3.1). The time of pressurization is determined by the mass of CO_2, the enthalpy difference and the heat leak:

$$dt = \frac{m\ dh}{Q_{leak}} \tag{10}$$

For de-pressurization, the emergency cooling system modifies the heat leak to a negative value, effectively subtracting the cooling capacity from the heat leak. The absolute value is taken to ensure the time remains positive:

$$dt = \left| \frac{m\ dh}{Q_{leak} - Q_{chiller}} \right| \tag{11}$$

2.5 Pressure Drop

In real moving fluids in a pipe, the pressure varies along its path. Equation (12) shows the composition of the overall pressure loss in real moving fluids. Friction between the fluid and the pipe's interior surface, as well as directional changes, enhance the frictional proportion of the overall pressure loss and act as a resistance to the flow. Major losses due to friction occur per unit pipe length, while bends, fittings and valves contribute a minor proportion respectively.

$$\Delta p_{total} = \Delta p_{frict} + \Delta p_{static} + \Delta p_{mom} \tag{12}$$

The static height head loss is of particular importance for this work, as the evaporator is significantly elevated relative to the condensing unit. This pressure drop arises due to the gravitational force acting on the fluid column, with the pressure increasing in downward flow and decreasing in upward flow, depending on the height difference between components. The definition of the static height pressure loss is given in Equation (13). In this equation, Θ represents the angle of the channel relative to horizontal, with a positive sign indicating an upward flow. Additionally, H is the height difference of the inlet and outlet of the considered pipe section.

$$\Delta p_{static} = \pm \rho_H\ g\ H\ sin\Theta \tag{13}$$

In this notation the homogeneous density, ρ_H, is considered. While the determination of the fluid density in single-phase flow is straightforward, it becomes more complex in 2-phase flow

due to the coexistence of vapor and liquid phases. The homogeneous density accounts for the vapor quality and is calculated as follows:

$$\rho_H = \left(\frac{x}{\rho_G} + \frac{1-x}{\rho_L} \right)^{-1} \tag{14}$$

Here, ρ_G represents the density of the vapor phase, ρ_L represents the density of the liquid phase, and x is the vapor quality, which denotes the mass fraction of vapor in the two-phase mixture.

The momentum proportion is not taken into account in this work, as it requires knowledge about the inlet and outlet conditions of the flow within the pipe section. Heat intake from the environment leads to a decrease in fluid density, which, to conserve mass flow, results in an increase in velocity proportional to the density reduction. The higher velocity enhances the flow's momentum. Thus, it can be concluded that the momentum pressure drop under a positive temperature gradient to the environment contributes positively to the overall pressure drop.

2.5.1 Darcy Weisbach Correlation

Equation (15) is the Darcy-Weisbach correlation, a common correlation to predict the friction-based pressure drop in single phase flows by knowing the velocity and the Darcy friction factor.

$$\frac{\Delta p_{frict}}{L} = f_D \frac{\rho}{2} \frac{\langle v \rangle^2}{D_H} \tag{15}$$

The implicit Colebrook-White equation (16) is applied for evaluation of the friction factor. This equation has an effective range of $4000 < Re < 10^8$ for single-phase flow (Brown 2002).

$$\frac{1}{\sqrt{f_D}} = -2 \log_{10} \left(\frac{e}{3.71\, D_h} + \frac{2.51}{Re \sqrt{f_D}} \right) \tag{16}$$

The static height equation (13) contributes to the overall pressure drop with a negative sign, as the flow's direction is simplified to vertical downward and supported by the gravitational force. The rearranged summation (17) illustrates this relationship. When the negative notation of the angle is taken into account, the term enters the equation as a positive addend.

$$\Delta p_{frict} = \Delta p - \Delta p_{static} \tag{17}$$

Equation (18) shows the rearranged Darcy-Weisbach correlation considering the static height pressure drop.

$$v = \sqrt{\frac{2\ (\Delta p - \rho\, g\, h\, sin\Theta)\ D_H}{f_D\, L\, \rho}} \tag{18}$$

$$v = \sqrt{\frac{2\ (\Delta p - (-\rho\, g\, h\, sin 90°))\ D_H}{f_D\, L\, \rho}} \tag{19}$$

The momentum pressure drop is not considered, as the inlet and outlet conditions are assumed to be equal and thus, the density is constant along the pipe length.

2.5.2 Friedel Correlation

For estimating the frictional pressure drop in 2-phase flow, considering the phases separately has been demonstrated in the past to give reliable predictions. The separated flow model was initially introduced by Lockhart and Martinelli in 1949 and later expanded upon by numerous researchers. These models are based on the assumption that the velocities of each phase remain constant in the occupied fraction of the cross-sectional area. Schmid et al. 2022 compared widely used models and categorized in applicability across various vapor qualities and pipe diameters in vertical upward flows. Among these models, the Friedel correlation demonstrated its validity as a reliable candidate for predicting two-phase pressure drop for CO_2 and a wide range of pipe diameters.
The Friedel correlation, (20), utilizes a 2-phase multiplier to account for the deviations from single-phase (liquid) pressure drop.

$$\Delta p_{frict} = \Delta p_L \, \Phi_{fr}^2 \tag{20}$$

The frictional pressure drop caused by liquid flow is calculated as:

$$\Delta p_L = 4 \, f_L \, \frac{L}{d_i} \, \dot{m}_{total}^2 \, \frac{1}{2\rho_L} \tag{21}$$

The liquid friction factor f_L and the Reynolds number are obtained from:

$$f = \frac{0.079}{Re^{0.25}} \tag{22}$$

$$Re_L = \frac{\dot{m}_{total} \, d_i}{\mu_L} \tag{23}$$

utilizing the liquid dynamic viscosity μ_L. The 2-phase multiplier itself is defined by:

$$\Phi_{fr}^2 = E + \frac{3.24 \, F \, H}{Fr_H^{0.045} \, We_L^{0.035}} \tag{24}$$

E, F and H are dimensionless factors:

$$E = (1-x)^2 + x^2 \, \frac{\rho_L \, f_G}{\rho_G \, f_L} \tag{25}$$

$$F = x^{0.78} \, (1-x)^{0.224} \tag{26}$$

$$H = \left(\frac{\rho_L}{\rho_G}\right)^{0.91} \left(\frac{\mu_G}{\mu_L}\right)^{0.19} \left(1 - \frac{\mu_G}{\mu_L}\right)^{0.7} \tag{27}$$

as well as the Froude (Fr), which states the relation of flow inertia to the external force field:

$$Fr_H = \frac{\dot{m}_{total}^2}{g \, d_i \, \rho_H^2} \tag{28}$$

and Weber (We) numbers, providing the relation of fluids inertia to the surface tension:

$$We_L = \frac{\dot{m}_{total}^2 \, d_i}{\sigma \, \rho_H} \tag{29}$$

For the homogeneous density, ρ_H, the following equation is used:

$$\rho_H = \left(\frac{x}{\rho_G} + \frac{1-x}{\rho_L} \right)^{-1} \tag{30}$$

Thome n.d. recommended this procedure for $\frac{\mu_L}{\mu_G} < 1000$ and it is applicable for $0 \leq x \leq 1$. Since the Friedel correlation is used to predict the pressure drop based on known parameters, such as the total mass flux ($\dot{m}_{total}$), and pressure drops are obtained from the tests, this equation can be rearranged. As the rearranged formula is implicit, the results were obtained iteratively, using Python.

3 Design

In case of a primary chiller failure, a redundant subsystem must overtake the cooling functionality. The goal is to keep the pressure in the vessel below 45 bar, its design pressure. Therefore the heat absorbed in the thermosiphon and the heat leak across the vessel's insulation must be removed from the system. An emergency cooling subsystem must be integrated to quickly decrease the temperature, and thus the pressure, when the pressure goes beyond the desired threshold operated by a pressure switch mechanism.
The chapter covers the following points:

- Heat leak evaluation and the resulting pressurization to determine the desired cooling capacity
- Defining the requirements for an emergency cooling subsystem
- Decision-making process on whether to buy or build the safety cooling subsystem
- Explanation of the chosen cooling system's functionality and its components
- Specifications of the design: Pipe sizing and material selection, expansion device, pressure supervision and actuation system and the heat exchanger for the vessel

3.1 Heat Leak Evaluation

The heat loss to the ambient is being assessed here, starting with the heat leak across the insulation and walls of the vessel. Since the surface storage vessel is integrated into the system, an additional proportion contributes to the overall heat leak: the thermosiphon loop's heat absorption. The loop is constantly circulating CO_2, pumping it from the underground plants to the surface storage. The loop's piping consists of vertical and horizontal sloped sections, resulting in over $400\,m$ of insulated pipes. The vessel is a double shell design with a thick layer of evacuated perlite in between. As the pipes provide a large surface, it is expected to have a pronounced impact on the overall heat leak, compared to the vacuum-insulated vessel on the surface. To understand the thermal dynamics of the system, the heat leak of the vessel and the piping assembly will be calculated and compared for the expected operational temperature range present inside the vessel.

3.1.1 Heat Leak of the Vessel

The vessel consists of a double-wall shell with the gap between the layers filled with evacuated perlite insulation.
The following assumptions were made for the calculation:

- The shape is assumed to be cylindrical, corners are neglected.
- Heat transfer due to radiation is considered negligible because of the vacuum insulation.
- The thermal conductivity of evacuated perlite ranges from 2 to 40 mW $m^{-1}K^{-1}$ at pressures from 1.3e^{-6} to 0.13 bar at -20°C (Lang et al. 2016).The highest conductivity value is selected for the heat leak calculation.

Table 1: Thermal and material properties for the calculation of vessel heat leak

Parameter	**Value**	**Unit**
Thermodynamic Properties		
Ambient temperature	$T_{amb} = 22$	$[°C]$
Temperature of CO_2	$T_{CO_2} = -35$ to 10	$[°C]$
Thermal conductivity (steel)	$\lambda_{steel} = 15$	$[W/mK]$
Thermal conductivity (Perlite)	$\lambda_{perlite} = 0.04$	$[W/mK]$
Heat transfer coefficient (outside, natural convection)	$\alpha_{nat} = 5$	$[W/m^2K]$
Heat transfer coefficient (inside, liquid phase)	$\alpha_{CO_2\,liq} = 100$	$[W/m^2K]$
Geometric Properties		
Insulation thickness (Perlite)	$\delta_{Perlite} = 219$	$[mm]$
Vessel 1 inner diameter	$d_{1,i} = 1,700$	$[mm]$
Vessel 1 outer diameter	$d_{1,o} = 1,750$	$[mm]$
Vessel 2 inner diameter	$d_{2,i} = 2,188$	$[mm]$
Vessel 2 outer diameter	$d_{2,o} = 2,200$	$[mm]$

Figure 12 displays the results of an initial calculation. Due to the minor influence on the total heat leak, the calculation is not refined here.

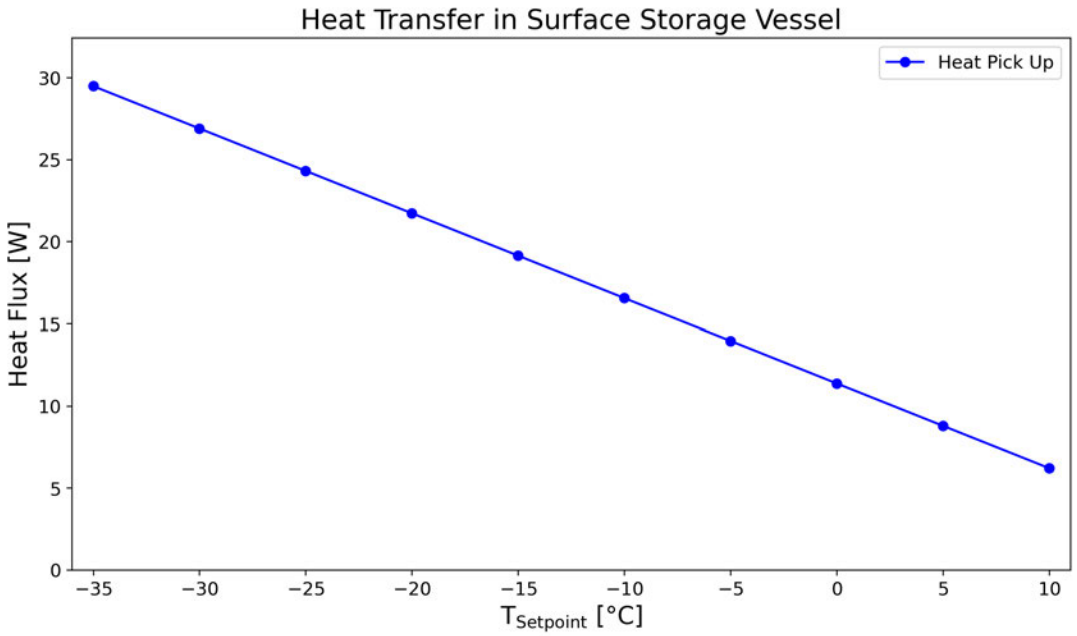

Figure 12: Calculation of heat leak to vessel

3.1.2 Heat Leak at the Thermosiphon

The thermosiphon loop consists of 440 m of insulated steel pipe and the design mass flow is 200 g s^{-1} (Verlaat 2023).While the temperature in the duct is expected to be constant, the temperature inside the pipe is dependent on the operational setpoint of the storage vessel. The calculation must display all possible scenarios. Table 2 is a list of the values used to calculate the heat leak.

The flow was simplified to assume a saturated liquid, disregarding the fact that the thermosiphon loop is subcooled in the downstream section and may be saturated or even 2-phase in the upstream pipe, which is essential for the natural circulation. The neglected temperature difference is the amount of subcooling. However, the temperature difference, as the main driving force for heat transfer, is small, but not specified yet.

The total heat pick-up is the sum of the calculated values for the supply and return line, as shown in the results displayed in Figure 13.

Table 2: Overview of values and properties for the thermosiphon loop's pipe assembly for the heat leak calculation

Parameter	Value	Unit
Thermodynamic Properties		
Ambient temperature	$T_{amb} = 22$	$[°C]$
Temperature of CO_2	$T_{CO_2} = -35$ to 10	$[°C]$
Pressure of CO_2	$p_{CO_2} = p_{sat}(T_{CO_2})$	$[bar]$
Vapor quality of CO_2	$x = 0$	$[-]$
Mass flow of CO_2	$\dot{m} = 200$	$[g/s]$
Thermal conductivity (Armaflex)	$\lambda = 0.04$	$[W/mK]$
Heat transfer coefficient (natural convection)	$\alpha = 5$	$[W/m^2K]$
Geometric Properties		
Insulation thickness (Armaflex)	$\delta_{Armaflex} = 50$	$[mm]$
Inner diameter of DN50 supply pipe	$d_{i,DN50} = 46$	$[mm]$
Outer diameter of DN50 supply pipe	$d_{o,DN50} = 50$	$[mm]$
Inner diameter of DN25 return pipe	$d_{i,DN25} = 27.2$	$[mm]$
Outer diameter of DN25 return pipe	$d_{o,DN25} = 33.7$	$[mm]$
Length of DN50 supply pipe	$L_{DN50} = 220$	$[m]$
Length of DN25 return pipe	$L_{DN25} = 220$	$[m]$

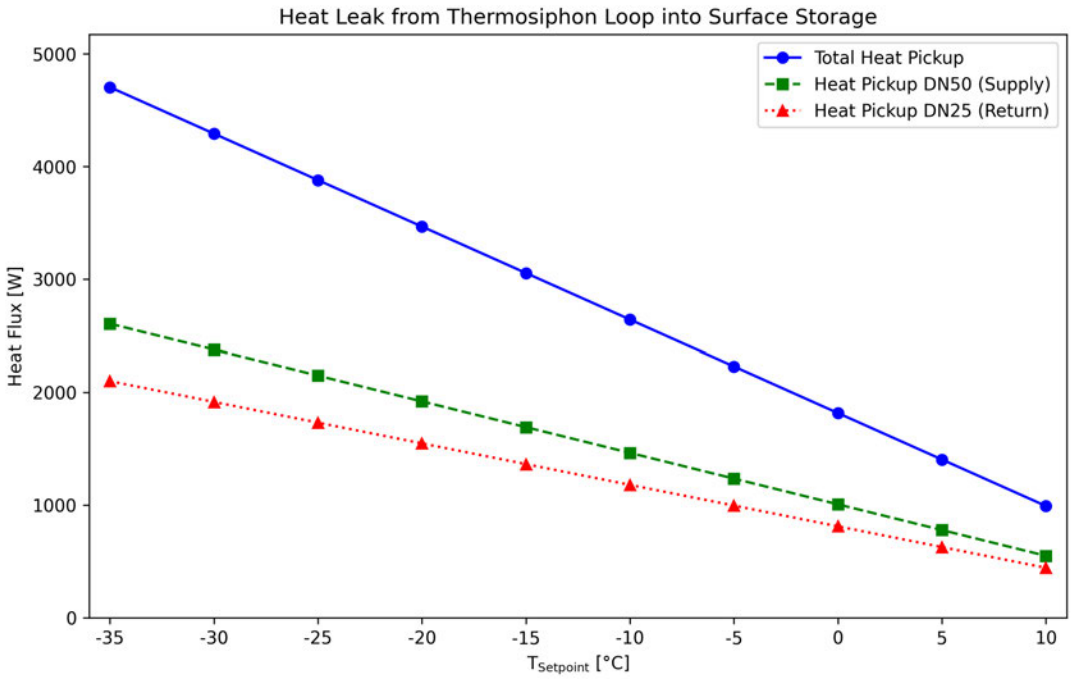

Figure 13: Calculated heat pick-up of thermosiphon loop piping

3.1.3 Conclusion

Comparing the heat leak through the vessel's walls and insulation to the heat pick-up of the thermosiphon loop yields a clear conclusion: the vessel's heat leak is negligible in terms of the safety cooling system's capacity. The heat leak of the vessel itself is below 50 W, whereas the thermosiphon loop can contribute up to 5 kW at the lowest temperature setpoint. A refined calculation could include heat leak at different fill levels, interfacial heat transfer of vapor and liquid phases and further adjustments to the heat transfer coefficients. Additionally, the assumption that return and supply line are at the same temperature, would slightly increase the heat flux to the ambient. Since the vessel's contribution to the overall heat leak is minimal and the temperature assumption in the thermosiphon loop only deviates slightly from operational conditions, no further refinement of the calculation is performed.
The heat leak from the thermosiphon piping is between 1 to 5 kW, depending on the setpoint, and must be covered by the safety cooling system for pressure control.

3.2 Design Requirements / Specification Sheet

Table 3 shows a summary of the specifications for the safety cooling subsystem.

Table 3: Design requirements for the safety cooling subsystem, categorized as ”Must Have”, ”Essential”, and ”Preferable” for clarity.

Requirement	**Priority**	**Reason**
5 kW cooling capacity	Must Have	Inevitable to meet the cooling requirement.
Ability for immediate activation	Must Have	Required to ensure rapid response in emergency conditions.
Reliable system, minimal electrical control, mechanical solutions	Must Have	The system must be dependable with minimal complexity, focusing reliability.
Suitability to large height difference	Must Have	Evaporator mounted in 9 m elevation.
Fit underneath shed	Must Have	Space constraint, unlikely to exceed due to small capacity
Evaporating temperature below 10°C, preferably -15°C to -5°C	Essential	This ensures the desired cooling conditions for maintaining the vessel below 45 bar.
R744 as working fluid (CO_2)	Preferable	Environmental considerations, CO_2 is used elsewhere - well-known, established expertise.
Easy to operate, documentation (manual, troubleshooting guide)	Essential/ Preferable	Clear documentation ensures ease of use, maintenance, and troubleshooting.
Able to cope with outdoor weather conditions (year-round)	Preferable	Must function effectively in all seasons and under varying weather conditions or must be achievable through modification.
Flow in two-phase pipes >300 kg $m^{-2}s^{-1}$	Preferable	Ensures effective heat exchange and fluid transport under operating conditions, but can be adjusted by pipe sizing.
Low maintenance	Preferable	Frequent maintenance requirements may cause third-party involvement or organizational complications.

3.3 Detailed Design

The safety cooling system will utilize a vapor compression cycle with CO_2 as the working fluid. Naturally, two options present themselves for the components responsible for compression and condensation: a commercially available condensing unit or an in-house built system. While commercially available condensing units offer the advantage of being ready-to-use solutions, an in-house built setup provides the flexibility to tailor the system to specific requirements.

3.3.1 Condensing Unit (Buy or Build)

This chapter documents the decision-making process, weighing the advantages and disadvantages of each option to determine which is more feasible for the intended purpose. Table 4, a list of the advantages and disadvantages, is used as a methodological tool to systematically analyze the arguments. Yellow-marked cells indicate neutral (medium-level) arguments, while cells in green and red color highlight arguments in favor or against.

Table 4: Comparison of Purchased System and In-House Self-Built System

Category	Purchased System	Self-Built System
Cost	High initial cost	Potential hidden costs
Customization	Limited options	Highly flexible
Expertise Required	Minimal technical knowledge	Significant expertise needed
Time Investment	Quick delivery, testing	Time-intensive
Documentation	Available, with troubleshooting	Create an own
Reliability	High, with warranty	Depends on expertise
Learning Opportunity	Minimal	High, valuable technical skills
Integration	ON/OFF status monitoring	Customizable

The purchased units available on the market are compact systems, the customization is limited to the parts outside the black box such as the dimensioning of the piping and the expansion device. Tests will show, in what configuration the unit is best to implement. Also in a purchased unit, the cooling capacity is fixed. For self-built systems, components such as the compressor can be upgraded in need. However, the opportunity of upgrading the self-build system, adds uncertainties to the cost prediction. Same can be said for the purchased unit, if a unit does not perform well in the tests and a different model seems more suitable afterwards.

The cost of an off-the-shelf condensing unit is more predictable, as these units are pre-engineered for a certain range of pipe diameters and types of expansion devices. In contrast, a custom-build system requires extensive development, including design, commissioning and testing phases before assumptions regarding pipe dimensions and expansion device can be established. Potential hidden costs can be assumed in the iterative process of developing a custom-built safety cooling system. Collaborating with a contractor, who would be responsible for designing and commissioning, could mitigate some of these costs, leveraging the company's expertise in component integration. However, this approach does not ensure a less expensive solution than

buying a compact system off the market.

A similar consideration applies to the timeline: Purchasing a unit off-the-shelf is likely faster, than the process of developing a custom-built system. The testing phase of the custom-built unit focuses on all aspects of the system, while the purchased system's testing phase focuses more on the components outside of the unit once the operational principles of the controller are understood.

The off-the-market condensing unit's controller ensures stable operation, it is user-friendly and requires no engineering expertise to operate. In case of the purchased unit, the manufacturer might not disclose the program on the controller fully. However, the unit comes with a users manual, including troubleshooting documentation, which is highly desired for a safety system. The testing campaign aims to determine whether further technical insights are necessary to operate the purchased unit as a safety cooling system. In case of a self-built system, also the controller must be procured and set up. Development of a controller is an additional factor extending the schedule. After commissioning and testing the custom condensing unit system, a manual must be generated using the gained knowledge and the documentations of the components.

Considering that the condensing unit will be localized outside, underneath the surface storage, semi-exposed to the environmental conditions and seasonal precipitation, a protective housing must be included in the design of a self-built unit. A ready-to-use commercial unit is mostly available in a weatherproof box-like configuration.

For a self-built system, the existing controls environment of the surface storage serves as the foundation for choosing and programming a controller. In case of a purchased unit, integration into the main SCADA (Supervisory Control and Data Acquisition) system is necessary to enable real-time monitoring and data acquisition within the communication network. Since the back-up chiller is a stand-alone safety system, simplified supervision is sufficient. The pressure switch mechanism and a temperature or pressure supervision of the flow leaving the black box can already indicate operation status to the SCADA system.

The back-up chiller is a redundant safety cooling system, where reliability is the top priority. Replicating the development period and the engineering expertise invested in commercially available condensing units to achieve high reliability is a highly time-intensive effort. Market-available units, meet the specified requirements while also aligning favorably with costs and time considerations. Furthermore, the system's integration into the existing control environment was found to be feasible with a simplified approach: pressure and temperature readings on the outlet are sufficient to confirm the unit's operational status. Additional benefits of a pre-engineered purchased unit include comprehensive documentation of the system, troubleshooting manuals and the provision of a manufacturer warranty. These factors further contribute to a reliable and user-friendly solution. Given that the demands are adequately met by commercially available units, the need for a customized cooling system is not compelling.

Consequently, the decision is to procure a pre-engineered condensing unit rather than custom-built solution, ensuring proven reliability and efficient integration within the system constraints.

3.3.2 Market Research

This section presents the results of a market research conducted to identify suitable medium-temperature CO_2 condensing units for comparison. The units were evaluated based on their cooling capacities, evaporation temperature ranges, dimensions, and price. Unfortunately, height requirements were not specified or not in favor of the requirements and thus found not to be useful to include into the comparison. Whereas the minimum velocities to ensure proper oil transport were specified in some of the documentations. Table 5 summarizes the findings.

Table 5: Results of market research: Medium temperature CO_2 condensing units with liquid line receiver and flashgas bypass.

Manufacturer Model	**Capacity [kW]**	**T_{evap}[°C]**	**Price**	**Dimensions [mm]**
Danfoss Optyma iCO_2	4.58 @ -10°C, 5.90 @ +5°C	-15 to +5	€ 6241.50	1028x800x1500
SCM Frigo CUBO2 Smart MT030	2.6 @ -10°C, 3.8 @ +5°C	-15 to +5	€ 7900	803x617x1150
SCM Frigo CUBO2 Smart MT045	3.9 @ -10°C, 5.8 @ +5°C	-15 to +5	€ 7900	803x617x1150
Fischer [CF] NEO-M2	3.03 @ -10°C, 4.15 @ 0°C	-15 to 0	-	1028x390x1200

Each of the models presents itself as viable candidates, offering cooling capacities in the specified range, comparable pricing and suitable dimensions. The condensing unit by Danfoss stands out due to its strong performance across the range of evaporation temperatures, competitive pricing and the reputation of Danfoss as a trusted manufacturer. However, the performance of the Optyma iCO_2 at the required height difference must be evaluated through a testing campaign, as the specified maximum height difference of 5 m could impact its efficiency or oil transport.

The Optyma iCO2 has been selected as the preferred option, and its performance will be further investigated as part of the study.

3.3.3 Danfoss iCO$_2$ Condensing Unit

The Optyma iCO2 condensing unit by Danfoss is a single-stage transcritical vapor compression cycle. It is classified as transcritical because, dependent on the ambient conditions, the CO_2 is compressed above its critical temperature, as shown in Figure 15. A condenser is then called gas cooler because it is not only condensing but also cooling gas in a transcritical state.

Transcritical Refrigeration Cycle Heat rejection occurs above the refrigerant's critical temperature. It does not undergo a distinct phase change from vapor to liquid, it is in supercritical state. The critical point of CO_2 is at 31°C and 73.8 bar. It is at relatively low temperature, especially when considering effective heat rejection to environmental temperatures during summer. For conventional subcritical condensation during high pressure heat rejection, the ambient temperature must be low. In winter operation the ambient temperature is lower and a lower temperature of the refrigerant is sufficient for heat rejection. A distinct phase change occurs in the condenser. Operating a CO_2 condensing unit in summer at elevated temperatures, particularly when the ambient temperature is above the critical point, the temperature of the refrigerant required for heat rejection is in the transcritical region.

Cycle Description The operational scheme, displayed in Figure 14, shows the main components of the condensing unit under consideration, along with a downstream thermostatic expansion valve and an evaporator. Figure 15 illustrates the transcritical refrigeration cycle for CO_2 in the pressure-enthalpy-diagram, with the pressure plotted on a logarithmic scale. The numbering (1..7) is consistent through both figures. Starting from point (1), low-pressure hot gas is compressed, transitioned into either a subcritical or transcritical state dependent on the ambient temperature. The high pressure, high temperature gas is directed to the gas cooler (2) for heat dissipation to the ambient. A valve is metering the flow of the high pressure low temperature liquid (3) towards the receiver. The main purpose of the high pressure valve is to regulate the pressure in the gas cooler according to the ambient temperature and hence plays a key role in the transcritical operation decision.

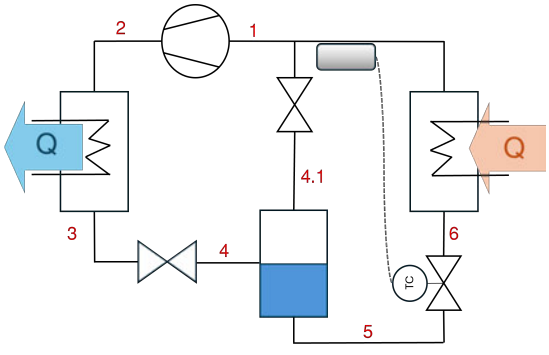

Figure 14: Danfoss Optyma iCO$_2$ operational scheme

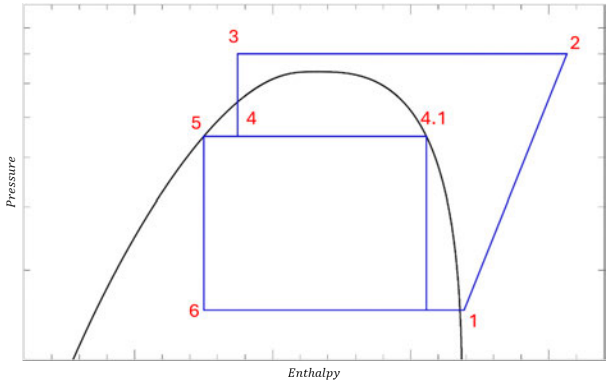

Figure 15: Transcritical refrigeration cycle CO_2 in a logp-h diagram

In the receiver, the 2-phase liquid is separated in vapor (4.1) and liquid (5) both in saturated

state. The liquid is sent to the outlet of the condensing unit in order to supply a heat exchanger with high pressure liquid. To maintain a constant pressure differential of 30 bar between the condensing unit's inlet, the suction line and the outlet, liquid line, and to ensure stable operation even during sudden load changes, the connected system or setup is bypassed by the receiver bypass valve. Here vapor (4.1) is metered to the suction line stream and hence the compressor inlet.

The connected system must include a throttling device upstream of the heat exchanger, expanding the liquid into the 2-phase state at lower pressure and temperature (6). In the evaporator, heat is transferred to the refrigerant and thus the enthalpy on the outlet (7) has increased. Initially, heat absorption causes a phase change, latent heat. Dependent on the heat load, heat can cause superheating, sensible heating. A liquid receiver, not displayed in the schematic, ensures only vapor entering the compressor in point (1), where the saturated vapor from the receiver is mixed in.

Condensing Unit's Operation The controller is regulating the compressor speed in accordance with the evaporator temperature requirement by means of the suction pressure: an up step in heat load at the evaporator leads to a rise in suction pressure. This is because the higher heat load increases the superheat and thus decreases the density at the evaporator exit. As a result, a higher volume of refrigerant is pushed into the suction port, increasing the suction pressure. The target difference in pressure is at 30 bar between the inlet and outlet ports of the condensing unit. Exceeding the target by 1 bar, the receiver valve opens and the compressor ramps up, the increased mass flow enhances the heat absorption at the evaporator and as a result, the suction pressure drops. Maintaining a fixed pressure drop across the connected setup including expansion device, piping and evaporator, provides a predictable and controllable system. As a result the pressure drop over the expansion valve is constant and the wear on the compressor is reduced due to less fluctuations in load requests. Also, the fixed dp has an positive impact on the heat rejection in the condenser of conventional vapor compression cycles. However, in transcritical cycles, like the Optyma iCO_2, a high pressure valve is present for pressure adjustments during heat rejection.

The fan speed for airflow across the gas cooler is also variable and regulated by the controller according to the required air-side convection to enhance the gas-cooling or condensation process.

High Pressure Control Valve The high pressure valve regulates the high-side pressure to its optimal value, fitting the operating condition, in order to achieve the best possible coefficient of performance (COP). In subcritical operation, the COP decreases as condensing temperature, and consequently the pressure rises. This is different in transcritical operation, where at a constant temperature of evaporation and gas cooler outlet the COP can increase and decrease with increase in heat rejection pressure, Eikevik 2023 (p.94).

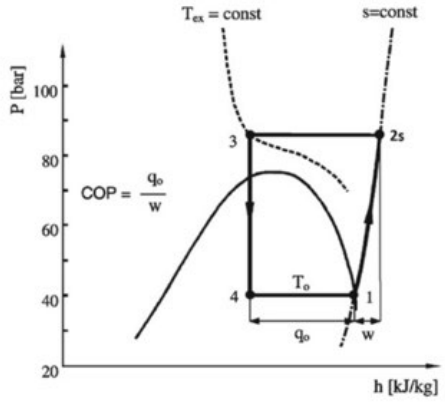

Figure 16: Transcritical isothermal and necessity of precise regulation of the pressure in the gas cooler for maximum COP (Eikevik 2023)

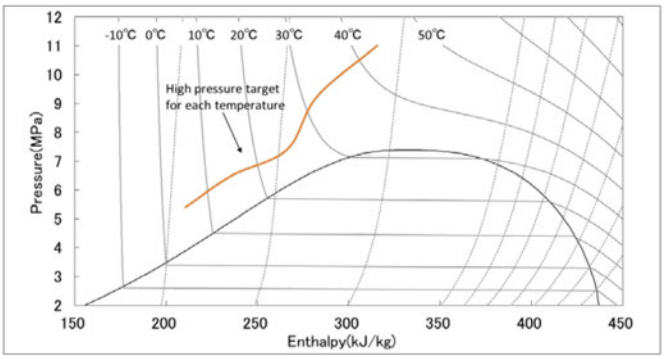

Figure 17: High pressure target dependent on gas cooler exit temperature displayed in a ph-diagram (*Optyma™ iCO2 condensing units - R744 | 50 Hz* 2023)

This is illustrated in Figure 16, where a simplified transcritical CO_2 refrigeration cycle is shown, in which T_{ex} is the temperature at the gas cooler exit. Due to the S-shape of the transcritical isotherms, a precise regulation of the pressure present in the gas cooler is required to achieve the maximum possible COP. The high pressure target, based on the gas cooler outlet temperature is illustrated in Figure 17, provided by Danfoss. Beginning in subcritical operation, the high-pressure target line indicates an increase in subcooling as the system approaches the transition to transcritical operation. This margin of subcooling ensures a smooth transition and helps to avoid the efficiency losses and instability typically associated with operating near the critical point. Following the high-pressure target line in Figure 17, an increase in gas cooler outlet temperature leads to higher vapor quality after isenthalpic expansion. As a result, the liquid proportion accumulating at the bottom of the liquid line receiver will decrease as the gas cooler exit temperature rises. Since the gas cooler outlet temperature is influenced by the environmental conditions, this process is limiting the overall performance during warmer months. Concluding is to say, that the relation of gas cooler outlet temperature and the pressure inside the gas cooler is a crucial factor transcritical in CO_2 refrigeration systems. Accurate prediction and precise control optimize system performance and maximize the COP.

Receiver / Regulation As explained in the cycle description, the liquid, high-pressure CO_2 is expanded over the high-pressure valve into the receiver, where it arrives in 2-phase state. Liquid refrigerant accumulates at the bottom from where it is drained, while vapor separates at the top and is directed to the compressor inlet by the receiver valve on demand. A closed receiver valve leads to an increase in pressure, also downstream of the tank and will result in higher mass flow to the evaporator and vice versa. However, the receiver valve is keeping the receiver pressure constant, even in dynamic load changes. That simplifies the control and stable operation of the expansion valves upstream of the evaporators, ensuring a proper expansion due to homogeneous pressure conditions, (Eikevik 2023, p.196). Additionally, the receiver valve helps maintaining the target dp of 30 bar, which further unifies the operational conditions. The ability to meet the target dp may be compromised by means of the environmental temperature.

While during summer operation, the bypass valve lets of pressure, in winter the capacity of the condensing unit decreases, if the condensing temperature falls below a certain threshold and the target pressure difference cannot be reached, even with the valve fully closed.

It also appears reasonable that bypassing vapor via the receiver valve, and thus ensuring uniform pressure conditions, helps prevent damage or strain on components due to pressure imbalances, whether sudden or static. For the compressor, this means metering vapor to the compressor inlet unifies the entering refrigerants conditions, aligning them to the designed operating pressure.
The key benefits are as follows: receiver tank pressure control enhances stability in dynamic operations, resulting in predictable thermodynamic performance of the condensing unit and a quick response time to load changes. Additionally, maintaining uniform conditions protect components, such as the compressor from fluctuations.

Gas Cooler The multichannel design of the gas cooler inside the Optyma iCO$_2$ condensing unit is a compromise between heat transfer and pressure drop. Figure 18 shows the alloy multichannel tubes, presenting its small channels that cause the larger pressure drop while enlarging the effective area for heat exchange.

The refrigerant-side pressure drop reduces the efficiency by increasing the load on the compressor in order to reach a pressure target on the outlet. Meeting the target pressure, which is linked to the ambient temperature, is contributing to the overall efficiency. The system expects to reject heat close to the ambient temperature and therefore sets a specific pressure on the compressor outlet. A decrease in pressure would reduce the heat rejection efficiency, as the temperature gradient is larger than predicted by the algorithm inside the controller.

Figure 18: Cross-sectional view of multichannel heat exchanger (Danfoss 2023).

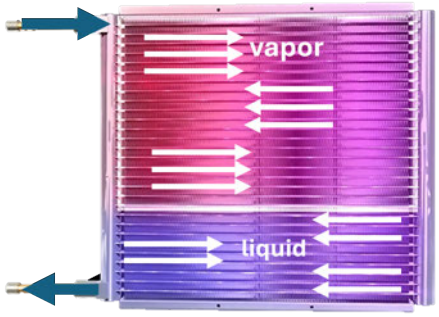

Figure 19: Qualitative representation of the flow distribution across a multichannel gas cooler, arrows indicate the pass-distribution (Danfoss 2021)

Noted by Eikevik 2023 (p.114), the flat geometry of the microchannel tubes have benefits, compared to round tube design: refrigerant-side area is three times larger, higher velocities on the air-side and thus better heat transfer.
Figure 19 is a qualitative presentation of the flow distribution across the multichannel heat

exchanger. The top section is dedicated to the entering vapor, which is less dense than the liquid or transcritical fluid of lower temperature. Therefore the vapor section consists of more interconnected rows in flow direction, than the bottom 'liquid' section. The pass-distribution ensures a high average velocity.
The overall cycle performance and efficiency is affected by the pressure differential across the gas cooler. A higher dp increases the workload on the compressor and lowers the efficiency of heat rejection.

Compressor The compressor inside the condensing unit is an inverter-driven variable-speed scroll compressor, capable of operating at a speed range of 2200 to 6840 revolutions per minute (rpm). The variable revolution feature allows the compressor to match its capacity to the heat load applied to the evaporator. The controller dictates the speed according to the suction pressure, ensuring stable performance and efficiency.

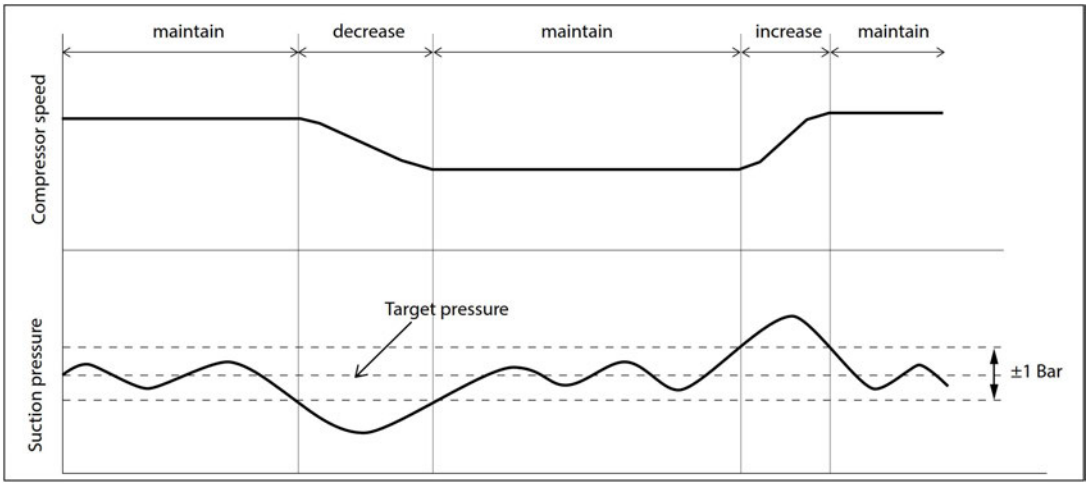

Figure 20: Compressor speed operation corresponding to changes in suction pressure (*Optyma™ iCO2 condensing units - R744 | 50 Hz* 2023).

To retain the oil, which bypassed the oil separator, the controller increases the speed according to an adjustable interval. Because the oil entrainment is a function of velocity, the controller intervenes once the compressor speed fall below a predefined threshold, set to 3000 rpm by default, for an adjustable time span, which is set to 20 minutes by default.

3.3.4 Oil Management in the Optyma iCO2

The insights of Section 2.2.3 regarding the oil management are referenced here to address the specific requirements of the Danfoss Optyma iCO_2 condensing unit.
The scroll compressor inside the condensing unit features an oil separator on the discharge port, but no sight glass for oil level monitoring. Consequently, there is no way to verify the oil level in the crankcase or the sufficiency of the oil transport.

The specifications provided by Danfoss must be followed with extra care:

- **Minimal downward slope** of 0.5% in horizontal pipe sections for returning flow.
- **Suction line velocity requirements:**
  - 4 m s^{-1} in horizontal sections
  - 8 to 12 m s^{-1} in vertical risers
- **Oil trap** in vertical risers, longer than 2.5 m.
- **Pipe support** intervals of 1 m in horizontal sections to prevent sagging.
- **Large-radius bends** maintain oil transport by minimized flow resistance.

These guidelines are critical for achieving stable and efficient oil management within the system.
The condensing unit's oil is a ND-8 Polyalkylene Glycol (PAG) provided by Denso. In B.V 2022, the supplier company, classifies the ND-8 as an ISO 46 (International Organization for Standardization) viscosity grade, which indicates a kinematic viscosity of 46 $mm^2\,s^{-1}$ at 40°C. The ND stands for non-detergent and indicate the absence of additives such as carbon removers, which is essential for maintaining the oil's purity and preventing unwanted chemical reactions in the system.
The chemical structure of PAG oil, shown in 31 and 32, consists of three sorts of molecules: alcohol ([R-OH]), ethylene oxide ($[EO]_n$) and propylene oxide ($[PO]_m$). The ND-8 PAG is double end-capped by [R-O] molecules, which makes it chemically inactive and stable. This property enhances its resistance to moisture as water molecules are less likely to bind to the chain, ensuring long-lasting lubrication performance.

$$\text{Single end-capped PAG chain: } \boxed{\text{R}} - [\text{EO}]_m\,[\text{PO}]_n - \text{OH} \tag{31}$$

$$\text{Double end-capped PAG chain: } \boxed{\text{R}} - [\text{EO}]_m\,[\text{PO}]_n - \text{O}\boxed{\text{R}} \tag{32}$$

Polyglycols (PAG) do not form varnish while wearing out, like comparable lubricants. Additionally, Nunez et al. 2008 found in their experiment, that the viscosity of polyol ester (POE), an often discussed alternative, degrades in CO_2 environment, due to its solubility. In contrast, PAG exhibited stable performance, making it a reliable choice for CO_2 refrigeration systems.
However, PAGs have a drawback — they tend to attract water, which compromises their lubrication ability and protection from corrosion. To address this, PAG fluids are blended to balance water and hydrocarbon solubility properties based on the application's needs (Perry 2018).
While miscibility is fortunate in terms of oil return to the compressor, a high miscibility can cause the viscosity to drop, and thus affect the lubricating characteristics. Ikeda et al. 2004 showed in his work, how PAG is a suitable lubricant and despite its lower miscibility did not show oil return issues.
Since the oil is in contact with electrical components, such as the compressor's motor coils, the dielectric strength of PAG is a further advantage.
In conclusion, PAG proves to be a suitable choice for CO_2 systems, as evidenced by the literature. Studies have demonstrated its reliable performance, resistance to viscosity degradation, the successful oil return, even with comparable lower miscibility, making it a reliable option for CO_2 refrigeration applications.

3.3.5 Refrigerant Charge

Danfoss specifies the CO_2 purity grade of 99.995% and a H_2O proportion less than 5 ppm for the system charge. The charge is to be calculated, considering the system volumes. Relevant for the calculation are the evaporator's volume, pipe size and lengths and the evaporation temperatures:

- Condensing unit: 2.15 kg of CO_2 to run properly
- Liquid line: 0.80 kg/L of CO_2, corresponding to 0.04 kg/m for 3/8" liquid line.
- Evaporator: 0.25 kg/L at evaporating temperature of +10°C and 0.15 kg/L at -5°C

The total amount is the system charge and must be carefully calibrated. A undercharged system will not reach the receiver pressure target and result in restricted mass flow and impaired cooling performance. Conversely, overcharging a system will result in excessive pressure build-up and consequently, venting through the safety valves.
Achieving the correct charge is crucial, as also noted by Eikevik 2023, as the charge directly affects the condensing unit's capacity and operational stability.

3.3.6 Expansion Device

In vapor compression cycles, various types of throttling devices are used for expansion. The thermostatic expansion valve, a variable cross-section and mechanically controlled metering device, is selected for the design and the forehand tests, due to its flexibility in operational conditions.
The market research is narrowed down initially, by the refrigerant type. The thermodynamic properties of refrigerants differ and necessitate proper valve sizing. Danfoss offers the TE2, a thermostatic expansion valve for CO_2 with a MOP (Maximum Operation Pressure) bulb charge, limiting evaporating pressure to 5°C. The valve is equipped with an external pressure equalization port, an important feature, considering the expected high-pressure drop of the pipes due to length and height. Furthermore, the valve's capacity is customizable to an extent, as the orifice can be changed. The orifice sizing process is elaborated in Danfoss' manual (*Thermostatic expansion valve type TE2 for R744; Thermostatic expansion valve type TE2 for R744* 2023).
Danfoss provides in the same document a capacity table to evaluate the right orifice for a range of cooling capacities. In order to determine the right orifice from the provided table, a calculation follows, which is elaborated here.

$$\frac{Q_{requ}}{f_{sub} f_p} = Q_{selec} \tag{33}$$

The cooling capacity Q_{selec}, takes system-specific parameters into account, including the required expected cooling capacity required on the heat exchanger (Q_{requ}). The operating conditions are characterized by the evaporating temperature (T_e), condensing temperature (T_c) and the superheat (SH). Additionally, Danfoss provides a table with subcooling correction factors f_{sub} and distributor correction factor f_p.
Since the condensing unit is equipped with a receiver, T_c refers to the temperature of the saturated liquid within the flash tank and f_{sub} was set to 0.97, since the liquid within the receiver is

saturated. The receiver temperature was set to 20°C, as it corresponds to the saturation pressure near 58 bar. Considering the 30 bar pressure difference, the condensing unit maintains, an evaporation temperature around -10°C is expected in the evaporator.
The distributor correction factor was set to 1, for a dp of 0 bar, as no distributor is foreseen in the setup. The required cooling capacity corresponds to the calculated heat leak of 5 kW.

$$\frac{5\,kW}{0.97 \cdot 1} = 5.15\,kW \tag{34}$$

The absence of subcooling results in a correction of the capacity, that is to select. Danfoss specifies the operational envelope of the available orifices and the cooling capacity of orifice ”01” is plotted over the condensation temperature in Figure 21. The dashed trendline is the polynomial extrapolation to estimate the capacities at higher condensation temperatures, outside the specified range. The maximum value of this extrapolation is to be tested.

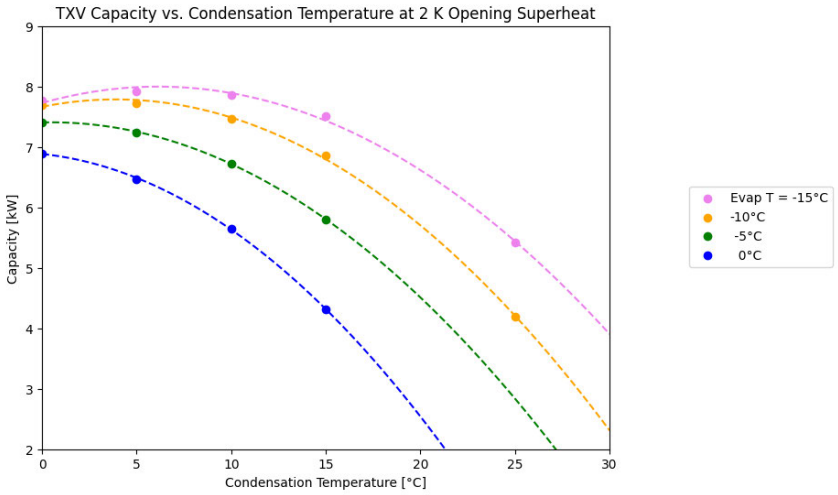

Figure 21: Extrapolation of capacity over condensation temperature for orifice ”01” available for expansion valve TE2 by Danfoss (*Thermostatic expansion valve type TE2 for R744; Thermostatic expansion valve type TE2 for R744* 2023).

In a vapor compression cycle with a flash tank or receiver, the condensation temperature corresponds to the receiver temperature of the saturated liquid. From this temperature, the throttling device expands the liquid into the two-phase region for evaporative cooling.
The cooling capacity decreases as the condensation temperature increases. This is because expansion from higher inlet temperatures at 0 K subcooling leads to higher vapor qualities and therefore higher enthalpy at the TXV exit. The latent heat the system can use for heat pick-up decreases at higher condensation temperatures, and hence the heat absorption capacity of the system, if opening superheat is constantly 2 K.

Expansion Valve Installation In Figure 22, the TXV and bulb are displayed, along with the copper strap to mount the bulb to the suction pipe. The TXV is installed on to liquid line upstream of evaporator and the bulb on the suction line as close to evaporator as possible for optimal information on heat exchanger utilization and for best stability. The bulb is to be installed on a horizontal pipe section, at a position between 10 o’clock and 2 o’clock, as shown

in Figure 23. Installing the bulb on the bottom of the return line bears a risk of malfunction due to accumulated oil, as it is corrupting the heat transfer. Furthermore, the bulb should only see suction temperature and must be protected against ambient conditions with insulation. To minimize latency in temperature change it must be installed in safe distance from large mass components. As the valve's head must always be warmer than the MOP-charged bulb, to avoid liquid accumulation and prevent malfunctioning (Eames, Milazzo, and Maidment 2014), the valve's head must be spared from insulation.

Figure 22: Thermal expansion valve (TXV) and bulb assembly, featuring the external equalization port and a copper strap for bulb installation (*Danfoss Refrigeration TXV* 2025).

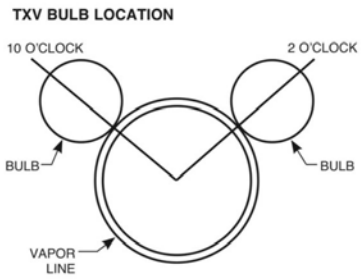

Figure 23: Installation of the bulb using a copper strap, showing the proper positioning (*Where to mount the TXV sensing bulb?* 2025).

3.3.7 Pipe Sizing

In order to supply the heat exchanger on top of the storage vessel sufficiently with refrigerant and ensure sufficient oil entrainment, the pipes must be sized accordingly. As the heat leak is evaluated, a calculation for an estimation of the flow inside the pipes of the supply and return lines can be performed. This will allow the evaluation of the pipe sizing and to a later point in this work a comparison to the acquired data from the tests.

This section begins by determining the cooling capacity at each evaporation temperature to later on calculate the required flow in order to remove the heat from the evaporator.

Capacity Evaluation With the enthalpy difference (Δh), including superheat, and the heat load (P) the required flow in the system can be analyzed. Since the saturated liquid from the receiver undergoes an isenthalpic expansion, this point represents the evaporator inlet enthalpy. The controller ensures adherence to the specified temperature setpoint, while the bypass valve maintains a pressure difference of $30\,bar$ between the receiver and the evaporator. This allows the inlet enthalpy to be directly determined from the p-h diagram for a given evaporating temperature. The outlet enthalpy of the isobaric evaporation accounts for the temperature increase

due to superheating, here set to $5\,K$. Table 6 shows the parameters obtained from the calculation.

Table 6: Parameters for velocity and mass velocity calculation for given evaporation temperatures, isobaric heat transfer, $SH = 5\,K$

Parameter	**Unit**	$T_{evap} = -15\,°C$	$-10\,°C$	$-5\,°C$	$0\,°C$
Receiver pressure	$[bar]$	52.91	56.49	60.46	64.85
Evaporation pressure	$[bar]$	22.91	26.49	30.46	34.85
Vapor quality inlet	$[kg\,kg]$	0.29	0.29	0.31	0.33
Enthalpy inlet	$[kJ\,kg^{-1}]$	244.97	253.84	264.06	276.28
Enthalpy outlet	$[kJ\,kg^{-1}]$	442.98	442.36	441.25	439.59
Enthalpy difference	$[kJ\,kg^{-1}]$	198.01	188.52	177.20	163.31

Single-Phase The superheated vapor in the return line and the liquid supply line before the TXV, are both carrying single-phase fluid. Since the thermodynamic properties and the mass distribution across the pipe diameter are uniform, the flow's quality is represented by its velocity. The first step involves calculating the mass flow rate ($\dot{m}$) by rearranging following expression:

$$P = \dot{m}\,\Delta h \tag{35}$$

The velocity of the fluid perpendicular to the cross-sectional area (A) can then be defined as follows:

$$\vec{v} = \frac{\dot{V}}{A} = \frac{\frac{\dot{m}}{\rho}}{A} = \frac{\dot{m}}{\rho A} \tag{36}$$

Pressure and enthalpy of the saturated liquid in the receiver and the superheated vapor allow to read out the densities (ρ) in order to calculate the velocities in the single-phase carrying pipes: the return line (superheated vapor) and the liquid line (high pressure, warm liquid).

Two-Phase For the two-phase flow exiting the TXV the velocity is not as indicative for cooling capacity. In two-phase flow characteristics, and thus heat absorption capability, change with vapor quality and flow. G, the mass velocity proved to be more successful at predicting cooling behavior. Equation (37) shows the calculation:

$$G = \frac{P}{\Delta h\,A} \tag{37}$$

The spatial distribution of phases in multiphase flow, like vapor and liquid in two-phase flow, is categorized in flow regimes. These regimes describe the characteristics of gas bubbles and liquid behavior in the flow. The specific flow regime depends on factors like tube size, orientation, geometry, and operating conditions, Kadish et al. 2022.
Schmid et al. 2022 were investigating flow patterns in a vertical upward flow at different temperatures and mass velocities in an $8\,$mm pipe. In vertical flow, gravity's effect on phase separation differs substantially from horizontal flows. The undesired stratified flow, in which the flow separates by density and thus liquid is traveling on the bottom of the pipe and vapor flows at higher

speed on the top, does not exist in vertical flow. Further, the authors found that in vertical upward flow of CO_2 with vapor qualities $x > / = 0.3$, a mass velocity of at least $300\,kg\,m^{-2}\,s^{-1}$ is fortunate for a churn flow pattern that transforms into annular flow with increasing vapor quality.

Results The calculated velocities are displayed in Figure 24 and the constraints are represented by the horizontal black dashed lines and the vertical line indicates the heat leak.

The liquid supply line velocity must not exceed $1\,ms^{-1}$ to prevent vibrations. Furthermore, Danfoss recommends a velocity of $> 4\,m\,s^{-1}$ in horizontal lines and $> 12\,m\,s^{-1}$ in vertical risers, to ensure sufficient oil transport in vapor-carrying pipes.

The velocities in the vertical vapor return line, where flow follows gravity and non-vertical sections sufficiently meet the requirement for horizontal line velocity with the $3/8$" tube. Additionally, this configuration provides velocities with a promising margin for operation.

Tests described in a later chapter will evaluate whether the resistance of a smaller return line will impact the overall performance.

The mass velocity in the supply line, carrying two-phase flow, is required to be more than 300 kg $m^{-2}s^{-1}$. This criterion is best met using the 3/8" pipe.

As the height and friction is not yet respected in this analysis, a higher flow rate might be required to account for resistances. Also, the heat leak to the environment, especially on the cold temperature 2-phase line, has not been included in this calculation. The heat leak might lead to an increase in vapor quality on the inlet of the evaporator. As a result the superheat rises and the TXV and condensing unit will try to compensate for the loss in efficiency, as cooling by superheating vapor is less efficient, than evaporative cooling.

Based on the theoretical results, the 3/8" pipe meets the requirements, and the 1/2" is not considered, despite the TXV outlet is of the larger diameter.

All calculations were carried out using Python, with fluid properties obtained from REFPROP (NIST).

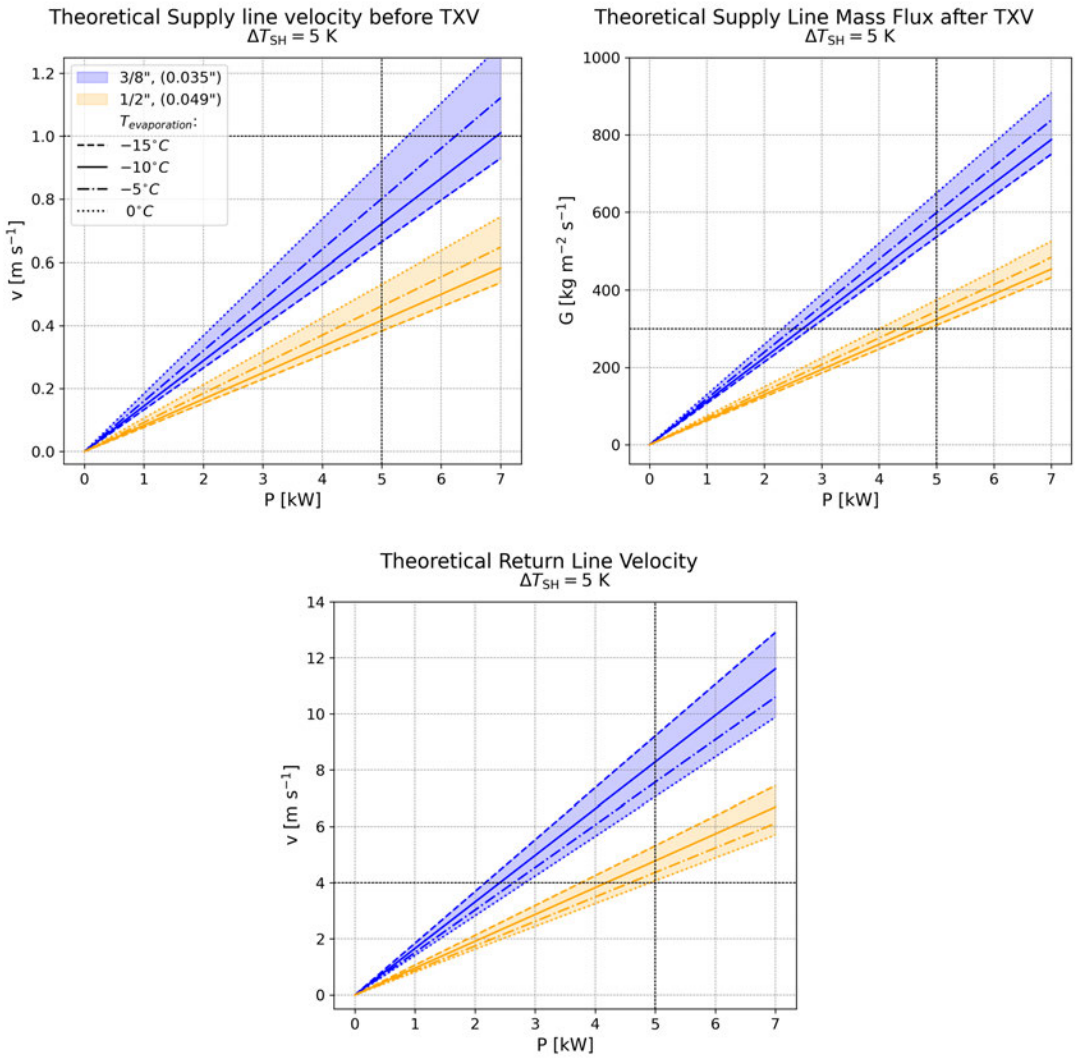

Figure 24: Results of theoretical velocity and mass flux calculation.

3.3.8 Pressure Switch

In order to activate the backup cooling system, a mechanism is required to detect when a specified threshold is exceeded. Once the chiller de-pressurized the vessel below a predetermined lower threshold, the unit switches off again. It is then meant to reactivate once the upper pressure threshold is exceeded. To prevent rapid oscillation between the on and off states of the emergency cooling system, a suitable pressure threshold must be defined. This threshold should be carefully selected, ensuring that the cooling system operates efficiently without unnecessary cycling.

A redundant mechanism must be selected to ensure reliable functionality without unnecessary complexity, as it is a critical safety feature. This redundancy can be achieved by incorporating simple, fail-safe components such as pressure switches with built-in hysteresis. Pressure switches, feature a mechanical diaphragm actuating an internal switch, reacting do power changes and thereby opening and closing the electrical connection according to an adjustable

hysteresis.

Diaphragm pressure switches are available in an adjustment range between 10 to 50 bar. The highest possible surface storage setpoint is at 40 bar. To allow for a margin between trigger pressure and design pressure, a pressure of 42 bar is a good fit for the upper pressure threshold. The hysteresis however, must be set in the factory and is selected in percent of the trigger pressure. Figure 25 shows the time of pressurization and the effect of the applied hysteresis of 10 % full scale on the depressurization by the 5 kW safety cooling system. The calculation according to section 2.4.2 is done for different setpoints and mass contained within the vessel. The time is calculated by assuming a homogeneous model, as described in the introduction.

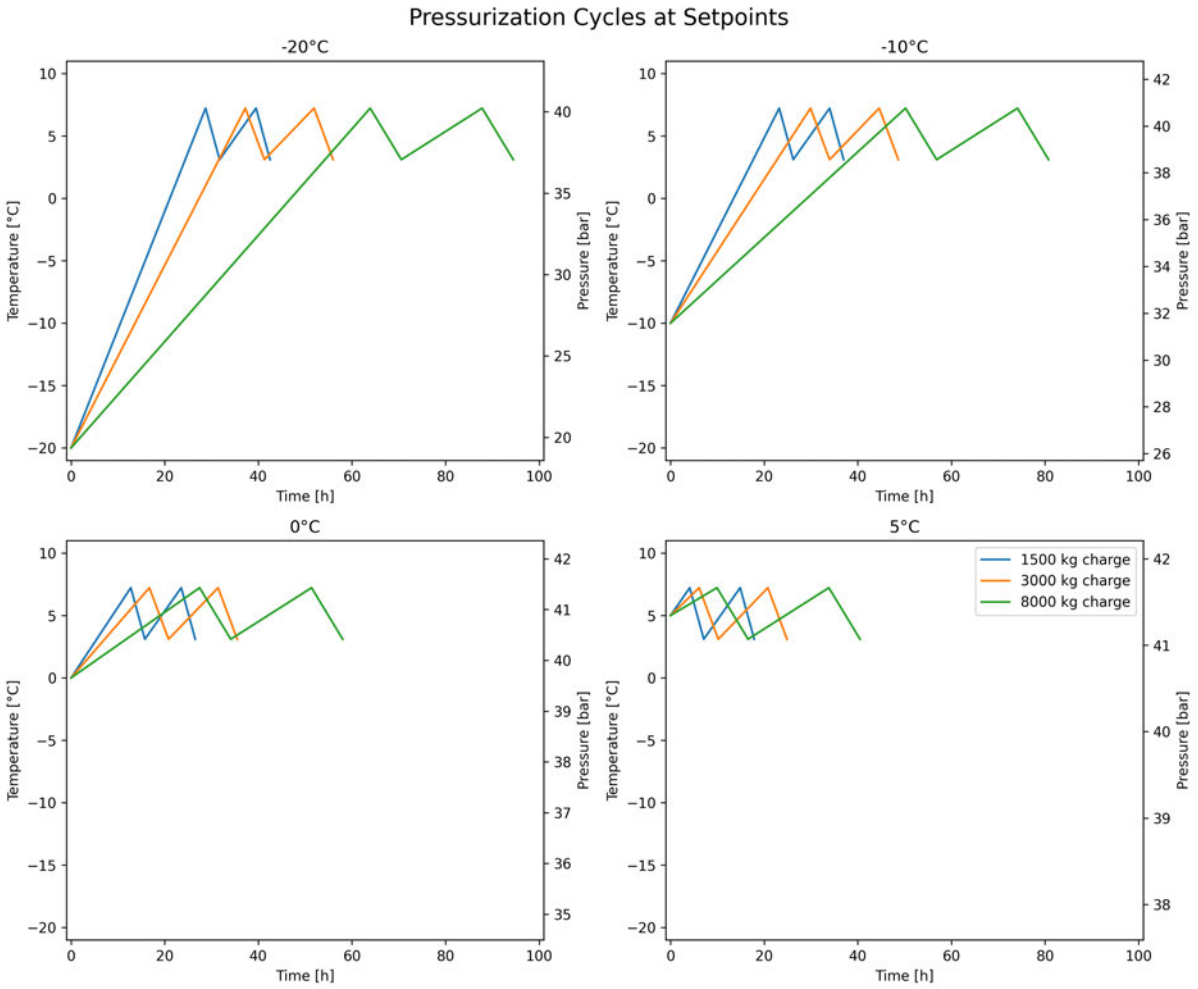

Figure 25: Pressurization cycles of the surface storage vessel due to the heat leak and cooling by a 5 kW cooling system, utilizing a pressure switch, triggering at 42 bar with 10% hysteresis.

One exception to the plot at 5°C is the fact, that if only the primary system fails, but not the heaters of the surface storage, the setpoint temperature will be maintained by heating. This is the case for all setpoints above the lower pressure threshold of here, 37.8 bar at 10% hysteresis and 42 bar upper threshold.

As demonstrated in the literature, prediction of the pressurization time by utilizing a homoge-

neous model provides an estimate of the slowest possible rate. However, this assumption is strengthened by the fluid motion induced by the thermosiphon piping, which is the dominant contributor of heat leak. However, the model neglects residual layer formation and interfacial heat transfer, which will have influence on the actual pressurization dynamics.

The hysteresis of 10% is recommended and a upper threshold well below the design pressure is chosen for possible start-up delays of the back up cooling system.

3.3.9 Heat Exchanger

The heat exchanger specified in the surface storage design, operated by the primary system, is a 50 kW brazed plate heat exchanger manufactured by SWEP. For the emergency cooling system, a heat exchanger with only 5 kW capacity is required. To maintain consistency and operational stability it is convenient to take the same type as specified for the 50 kW heat exchanger. Table 7 gives an overview of the BDW16DW heat exchanger's properties, proposed for the backup cooling system.

Property	**Value**	**Unit**
No. of plates	20	[-]
Heat transfer area	0.738	[m^2]
Heat transfer coefficient	555	[W m^{-2} K^{-1}]

Table 7: Properties of foreseen heat exchanger

4 Methods

In order to validate the design conclusions from Chapter 3, experimental data is required. This chapter outlines the test setup and testing procedure, that were used to determine the cooling capacity of the condensing unit as well as the performance of the chosen TXV. The evaluation assesses the suitability of this setup for the intended application scenario. Testing is particularly important since Danfoss specifies to not exceed a height difference of $5\,m$ between evaporator and condensing unit. The first phase of tests was conducted at ground level. This allowed for familiarization with the test setup and adjustments of procedures or setup before progressing to the more complex height test.
The test rig is constructed to replicate the real operating conditions as closely as possible. After commissioning of the setup in ground or height-level scenario, the system was evacuated to remove humidity and water. A leak test was performed and the setup was filled with the correct amount of CO_2 according to the calculation provided by Danfoss.

4.1 Test Setup

The setup consists of three main components: a dummy load, the thermostatic expansion valve and the condensing unit itself, residing on the ground. The P&ID in Figure 26 shows the three components in detail.

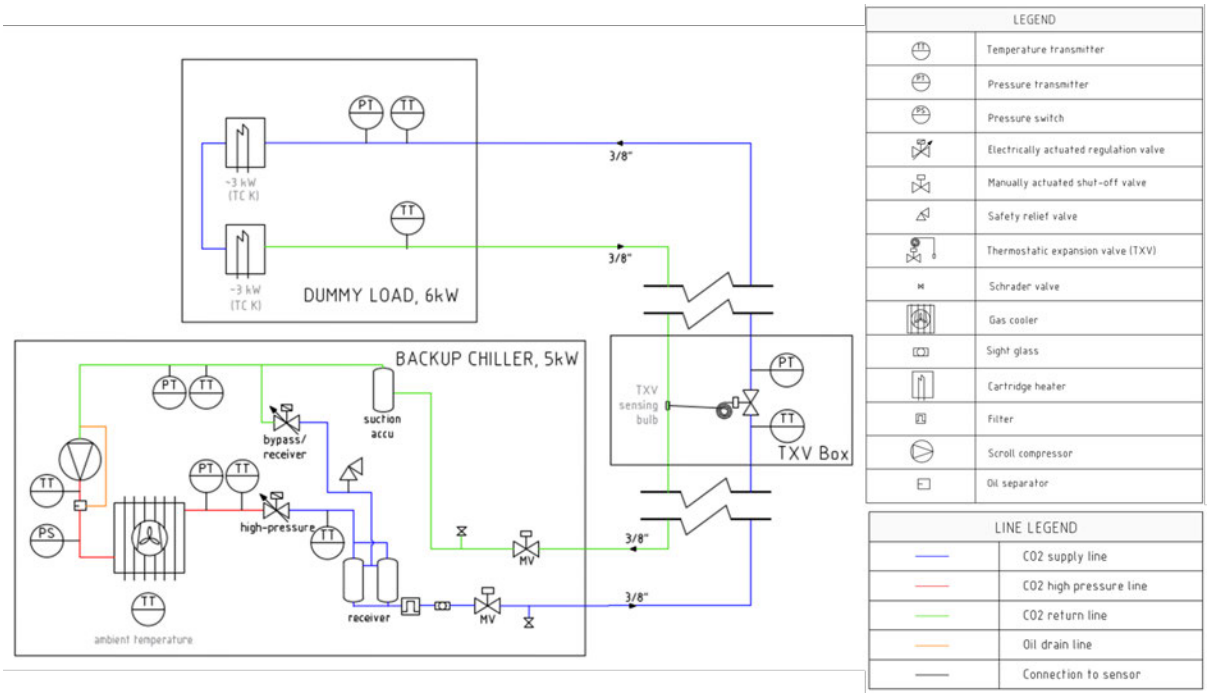

Figure 26: P&ID of the Optyma iCO$_2$ in conjunction with the test setup.

Dummy Load The dummy load is a transportable box of $140 \times 40 \times 20\,$cm and is representing the evaporator on top of the vessel. It is housing two 3-phase, 3 kW cartridge heaters inserted into a pipe assembly leaving the dummy load with an inlet and outlet port. The total heating power of 6 kW sufficiently represents the expected heat leak of the vessel with a margin. On

the inlet, pressure and temperature are monitored. An additional temperature sensor is located on the outlet for superheat detection. Both temperature sensors are mounted sideways into the pipe to prevent the tips from pointing into liquid phase at the bottom of the pipe. For the ground-level test, a second pressure sensor was monitoring the outlet pressure to determine the pressure drop across the dummy load. The core temperature of the heaters are supervised by temperature sensors, while two thermal switches are mounted to the surrounding pipe housing for safety.

TXV Assembly The TXV is contained in a box of $40 \times 40 \times 22$ cm. The TXV itself is located on the supply line and its equalization port is linked to the return line with a T-connection. The sensing bulb is mounted to the outside of the return line using a copper strap. For the height test, downstream of the TXV, a pressure sensor is monitoring the pressure on the TXV outlet and an oil check valve is installed on the horizontal section before the vertical long section. The boxes housing the dummy load and the TXV assemblies both are constructed of alloy profiles and the bulkhead and covers are made of G-10, a temperature-stable glass fiber resin laminate. The two boxes are insulated with caoutchouc foam.

Piping The piping utilizes 3/8” copper pipes with an inner diameter of 7.47 mm. The outlet of the TXV is reduced from 1/2” and ensuring uniform piping throughout the system. The general design prioritizes enhancement of oil transport and thus minimizing bends and slight slopes instead of horizontal sections. The pipes are insulated with polyethylene foam with a flame-retardant and weather-resistant low-density polyethylene jacket.

Control Cabinet A control cabinet houses the equipment necessary for electrical supply and system operation. The power controller regulates the input for the heaters. The Simex Multicon data logger is used for data acquisition of the sensor data from the test rig and within the condensing unit. The data logger acts as the master in the Modbus RS485 protocol, with the condensing unit as the slave, enabling steady communication. A voltage-free relay connection was implemented for enabling the thermostat mode testing. Further electrical equipment residing in the control cabinet ensures functionality and safety of the test setup.

Ground-Level Setup

- Condensing unit is placed on the ground.
- Expansion valve box and dummy load are elevated and positioned in a slight slope to prevent oil trapping.

Height-Level Setup

- Condensing unit is placed on the ground.
- Expansion valve box is hung up, with the outlet at a height of 3 m.
- Dummy load is placed 9 m high and positioned in a slight slope to prevent oil trapping.

Thermostat Mode Test The condensing unit's controller typically operates the system by monitoring the suction line pressure. When the suction pressure rises, the controller adjusts the cooling capacity in order to maintain the preset temperature setpoint. However, in the thermostat mode, the condensing unit is activated via a digital input, such as an evaporator thermostat, toggling through the voltage and allowing for on/off control. Once the unit is activated by the received digital signal, it again operates in pressure control mode, regulating the system based on suction pressure until the digital signal deactivates the unit.
The digital signal port on the terminal of the unit is bridged by default. Instead of using the default connection in the panel, a voltage-free switch or relay can be installed in order to toggle through the digital signal between the two ports.

4.1.1 Preparations

Subsequential to the commissioning of the setup the leak test follows. Therefore the condensing unit is put in ”vacuum mode”, during which all internal valves are opened. The system is pressurized with 50 bar of CO_2 and left idle for 12 hours. Changes in pressure should only be to observe due to ambient temperature variations. Once the system is leak tight, it is being evacuated. After evacuating the system for 4 hours the setup is charged with the setup-specific amount of CO_2 and oil. Oil was not added for both test conditions, since the evaporator and pipe volume do not exceed the threshold specified by Danfoss.

4.2 Testing Procedure

Two main testing procedures were conducted: the dynamic test and the long-term test.

- Dynamic Tests: In the dynamic tests, the heater power was gradually increased in steps, such as 1 kW increments, to obtain data at several setpoints and heat loads.
- Long-Term Tests: In the long-term tests, the power remained at a constant value for a time span of hours to days. After the tests over extended periods the unit and heaters were turned off and the system remained idle for 24 hours to allow any accumulated oil in the supply line to settle at the horizontal pipe, where the oil check valve is located.

The preset evaporation temperature was maintained consistently throughout each run of both test types.
Throughout the ground-level testing period, the superheat tuning of the TXV was evaluated. After each adjustment to the spindle, the same stabilization principle used in the dynamic tests was followed, as explained in the following. The built-in thermostat functionality was tested in the ground-level configuration.

Start-Up The test series begin with a structured start-up procedure. After powering up the condensing unit, the evaporation temperature setpoint is defined prior to switching the condensing unit to operation mode. To verify condensing unit operation, the inlet and outlet temperatures in dummy load must fall below ambient temperature. Once this verification is complete, the heat load can be applied to the heaters and the tests described in the following can be conducted.

Dynamic Tests Dynamic tests involved gradually increasing heating power and, consequently, cooling capacity in incremental steps.

Figure 27 illustrates the testing procedure and experienced system responses are plotted.

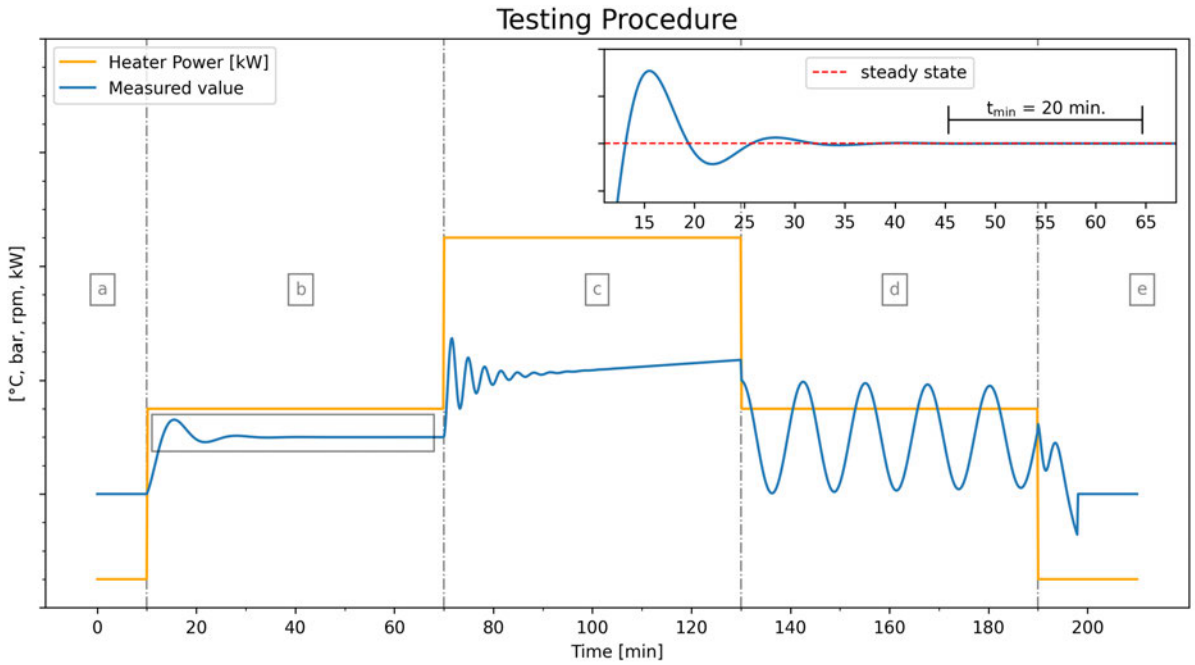

Figure 27: Testing procedure: Expected responses of an exemplary measured value to power changes. (a) Stable start condition, (b) Settling after overshoot feasible for data acquisition, (c) No steady-state possible (drift), (d) Oscillation without indication of settling, (e) Settling to a steady-state value.

After turning on the condensing unit and setting the evaporation temperature, it is necessary to wait for the measured value to stabilize. Section (a) represents the steady-state conditions of the desired parameter prior to the first power step-up. Following a power increase, the value might overshoot the steady-state value, as shown in (b), and eventually stabilize. A stabilization period of 20 minutes was considered sufficient for feasible data acquisition. After every successful step, the power was raised in increments, such as 1 kW. This process was continued until the maximum power was reached or the value was not stabilizing. In cases where no steady-state is achievable, a continuous drift might be observed, as shown in section (c). Data cannot be acquired, however, conclusions can still be drawn from these results. An example for an oscillating value without indication of settling is given in (d), no data can be acquired here either. The oscillations indicate hunting of compressor and expansion valve and thus, the test may be repeated at a later time. Section (e) shows, how a steady-state can be reached by changing the heater power, which was helpful to create a starting condition for further measurements. After observing a (d) scenario, where oscillations occur without any indication of settling, an (e) scenario is to strive for. This can be accomplished by a smaller-step approach to the power level of the prior (d) scenario, which proved to facilitate the establishment of a steady-state condition.

Long-Term Tests The long-term tests provided insights into the behavior of the condensing unit and expansion valve over extended periods of operation. Subsequently to the start-up procedure, the system was let idle at a constant heat load and temperature setpoint once a stable condition was reached, as shown in Figure 27(b).

Running the system for an extended duration allowed for observations on system stability and oil deposition. Eventually, a qualitative oil check was performed by opening the valve prior to the 6 m vertical section, downstream of the TXV.

TXV Tuning The impact and adjustment range of superheat tuning for the TXV were evaluated. The initial condition is a steady-state in the operational parameters such as the dummy load outlet temperature at a constant heat load and temperature setpoint. For assessment of the valve behavior, the setpoint and load were kept constant for the duration of the tuning tests. The tuning process involved turning the spindle by half a turn, which modifies the tension on the internal spring, thereby influencing the valve's response to temperature changes. After each adjustment to the spindle, a steady-state condition was aimed for, as shown in in Figure 27(b), where initial oscillations decrease and a stable operating point is reached.

Thermostat Mode Testing this functionality was performed to familiarize with the functionality of the thermostat mode. The unit was switched to operation mode and let stabilize at constant heat load and temperature setpoint. After switching the relay to the off position it was switched on again. Observations about the behavior were made from here on.

5 Results and Discussion

The results of the tests are discussed here. The differences between ground level and height test will be elaborated. In order to discuss the pipe sizing, the obtained pressure drops will be used for the calculation of velocities and mass flux, allowing a comparison of theoretical velocities and pressure drops.

5.1 Cooling Capacity

Figure 28 shows the obtained data points of the dummy load inlet and outlet temperatures plotted over the heater power, for the four tested evaporation temperature setpoints for the height and ground setup. Also displayed in the plots is the associated compressor speed to each temperature measurement. The data was obtained from the dynamic tests and from the long-term tests at steady-state condition.

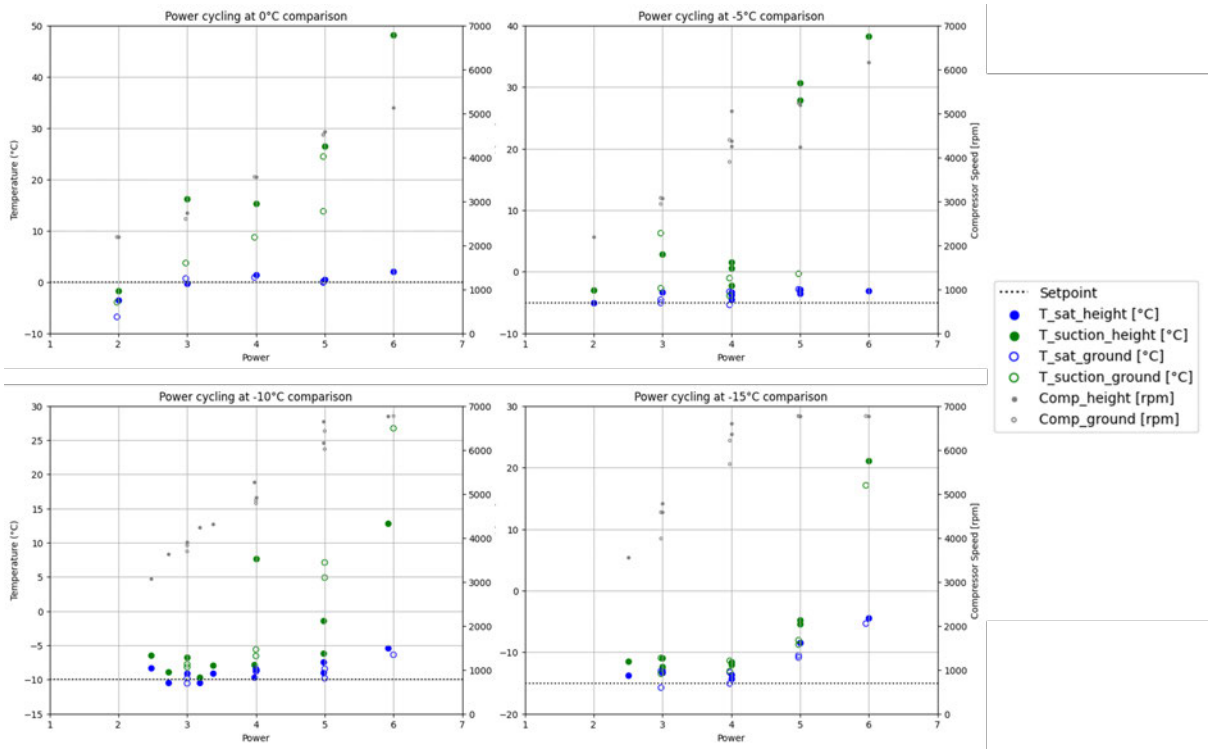

Figure 28: Plot of dummy load inlet and outlet temperatures, as well as compressor speed, at various evaporation temperature setpoints, with cooling capacity on the x-axis.

With increasing power, a linear increase in compressor speed is observed until it eventually stagnates at its maximum value. As the revolutions rise over power step-ups, the saturation temperature at the inlet is maintained and when the compressor reached its peak speed, the dummy load inlet temperature rises. Comparing the average compressor speed across the decreasing temperature setpoints, reveals an upward trend.
In Figure 29 the averaged evaporation temperatures from stable conditions obtained at the dummy load inlet in the ground setup and height setup test runs are displayed. The obtained measurements represent the operational envelope: While evaporation temperatures for the 0

and -5°C setpoints are relatively stable as the heating power increases, at lower evaporation temperatures, the deviations are increasing with power. Comparing the evaporation temperatures measured in ground setup and configuration with 9 m height difference at certain heat loads, no significant deviation is observed.

Also the minimal heat load of the test setup is clearly identifiable. During test runs at low heat loads, the condensing unit and expansion valve were causing oscillations.

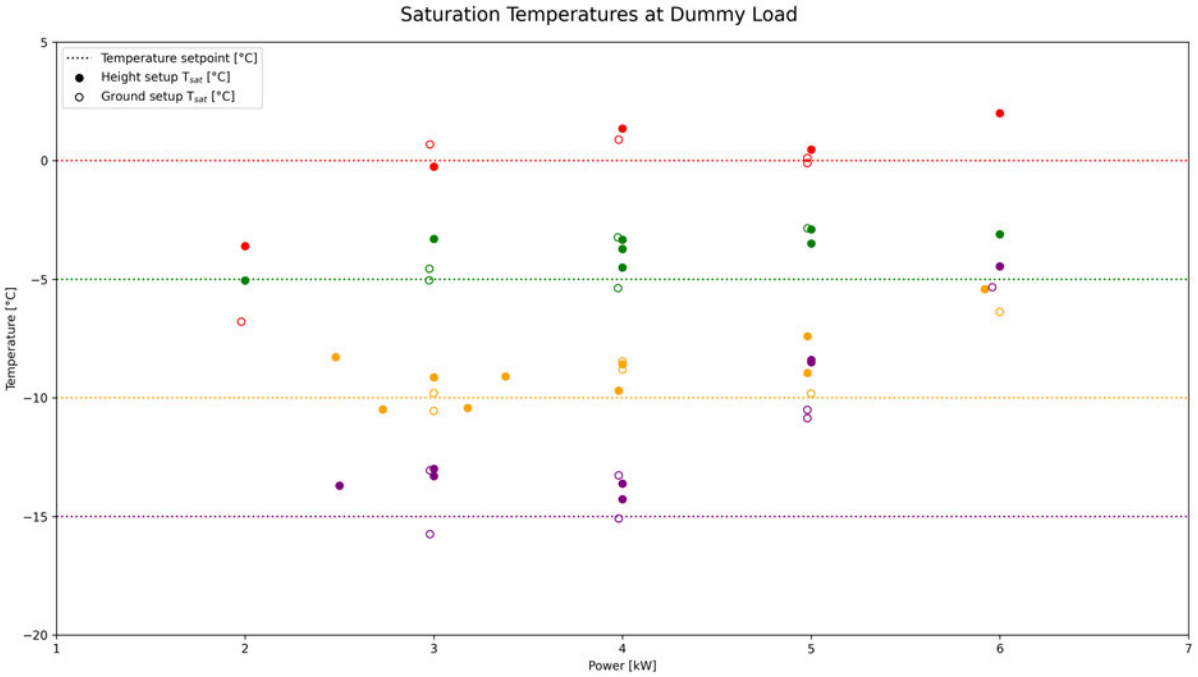

Figure 29: Comparison of the averaged saturation temperatures at stable conditions obtained from the height and ground setup test runs

Figure 29 shows the operational envelope, that is to expect for an application at height. Comparing the cooling capacities at height and ground level does not reveal striking deviations. The superheat at lower setpoints were more stable up until the heat load at which the capacity limit of the compressor and expansion valve are identifiable.

5.2 Thermostatic Expansion Valve

This section will briefly describe the results of the superheat tuning functionality. In Figure 30, a constant outlet temperature was aimed for by adjusting the superheat setting.

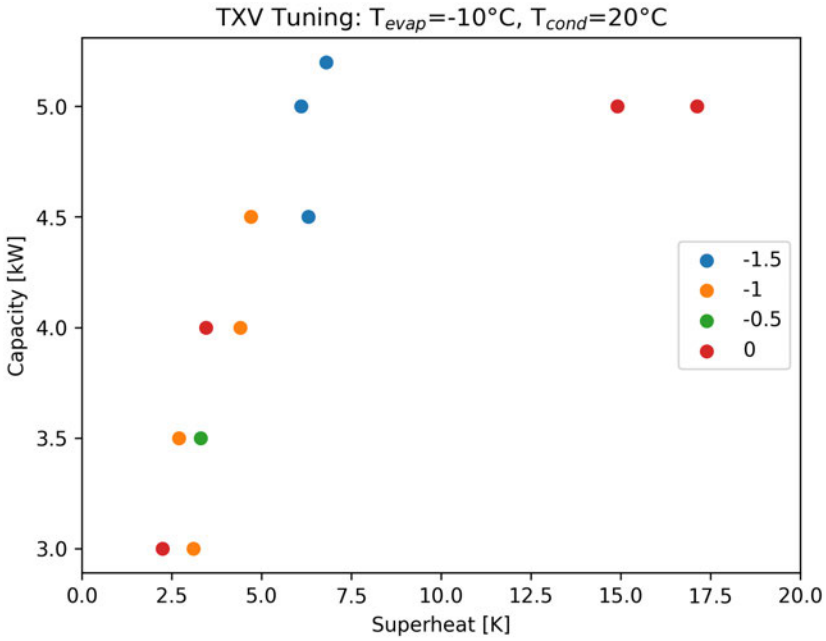

Figure 30: Overview of superheat tuning effect at evaporation temperature of -10°C and condensing temperature corresponds to receiver temperature.

The legend values in the figure represent the number of turns applied to the superheat adjustment spindle and 0 indicates the factory setting. The increase in superheat at rising heater power at factory setting is clearly to observe. The predicted rated capacity of approximately 5 kW at 5 K operating superheat in Figure 21, was only achieved by loosening the tension on the adjustment spring by 1.5 turns. The test was conducted during the ground-level testing phase, thus no influence of static height pressure drop or high frictional pressure drop due to long pipes.

5.3 Oil Entrainment

The oil transport across the system was found to be sufficient. Particularly in the rising 2-phase pipe, a bottleneck for oil transport was suspected, as it is the longest vertical section and oil transport capabilities vary with vapor qualities, hence flow patterns. A qualitative test was performed, to assess oil accumulation. After the first long-term test, a small amount of oil, in the range of 0.5 to 1 ml, was found in the pipe. The following two tests did not reveal any oil accumulation in the vertical supply line.
Although the dummy load was placed in a slight slope, with the inlet and outlet being the lowest points of the internal pipe assembly, it was searched for accumulated oil. After disassembly of the test setup the dummy load was placed vertically over seven days and no oil dripped out.

5.4 Thermostat Mode

The thermostat mode was tested as a proof of concept to evaluate its response and functionality. Upon the interrupted digital signal, the compressor stopped. Once the digital input was reactivated, the unit restarted, but only after a minimum delay of 180 seconds following shutdown. The delay is a preset parameter designed to prevent oscillatory start-stop cycles. During the shutdown, the pressure equalization inside the unit was to hear, as the receiver valve fully opens during shut-off.

5.5 Pressure Drop Investigation

The pressure drop is measured with the two Baker Hughes UNIK 5000 pressure sensors, one after the TXV and one on the dummy load outlet. For the UNIK 5000 the accuracy is specified as a percentage of full scale (FS), with the accuracy of ±0.10 % FS (150 bar) Best Straight Line (BSL). However, in the data sheet, information on the standard deviation or noise level of the sensor's output is not provided. The third pressure sensor is located inside the condensing unit, a Saginomyia HSK and its accuracy is specified as 1.0% FS (100 bar). When calculating the pressure drop using both sensors, the combined measurement error amounts to ±1.15 bar, affecting the data's absolute accuracy. However, comparisons can still be made to assess and evaluate trends. Despite the measurement uncertainty, the data remains valuable for drawing conclusions about the system performance and behavior.

Return Line Pressure Drop The pressure drops from the height setup and ground-level setup are displayed in Figure 31 for comparison. From the two measured pressure values, on the compressor inlet and the evaporation pressure in the dummy load, the pressure drop is calculated by subtraction.
The return line is governing a flow of superheated vapor. During the ground setup configuration, the pressure drop is purely frictional.

For the vertical downward flow, present during the height tests, the static height proportion adds to the overall pressure drop. The downward flow is aided by gravity and thus the measured pressure drop is the frictional proportion lowered by the amount of static head. However, the overall pressure drop is lifted by the friction proportion at height due to the long pipe and the influence of the static height proportion is rather small, caused by the low density of the returning vapor.

At higher evaporation temperatures and lower heater power, the setup exhibited reduced stability, making it difficult to obtain reliable and consistent data for acquisition. Consequently, these data points are less conclusive and should be interpreted with caution.

The pressure increase is expected to increase quadratically with power, assuming a constant superheat and thus constant enthalpy difference, since the pressure drop is proportional to square of velocity, as shown in the equation (15). Once the maximum speed is reached, the

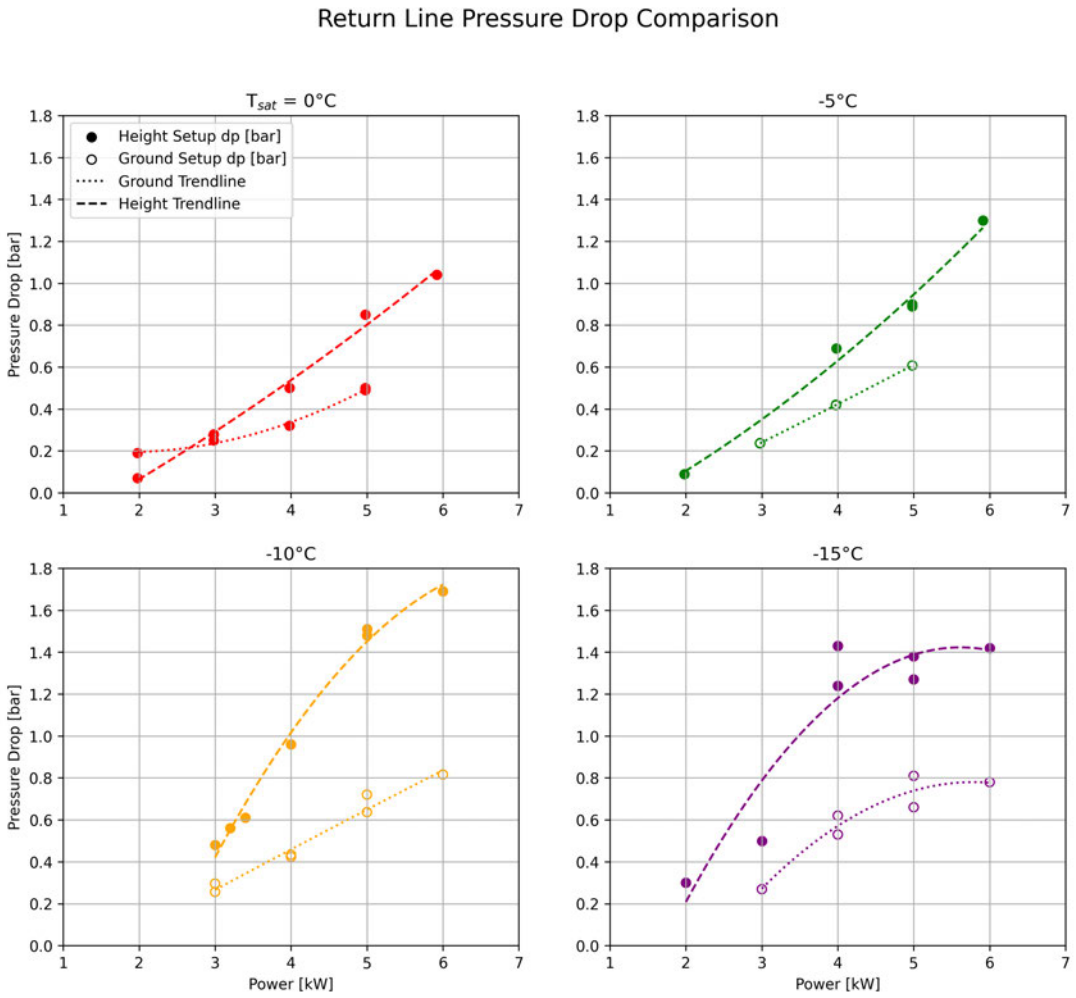

Figure 31: Measured pressure drop over heater power

pressure drop stagnates, as observed in the results presented in Figure 28. Visually, the pressure drop in both setups grow proportionally with increasing heater power for both, ground and height setup. However, at the lower evaporation temperatures (-10, -15°C), this trend eventually deviates from the expected increase or even stagnates at its maximum compressor speed and superheat and hence enthalpy difference increases.

Supply 2-Phase Line Pressure Drop The measured pressure drop and the calculated static height proportion are plotted over heater power in Figure 32.
A mostly proportional increase in pressure drop can be observed with increasing heater power. As the compressor speed increases, the frictional proportion rises, as higher velocity causes greater friction.

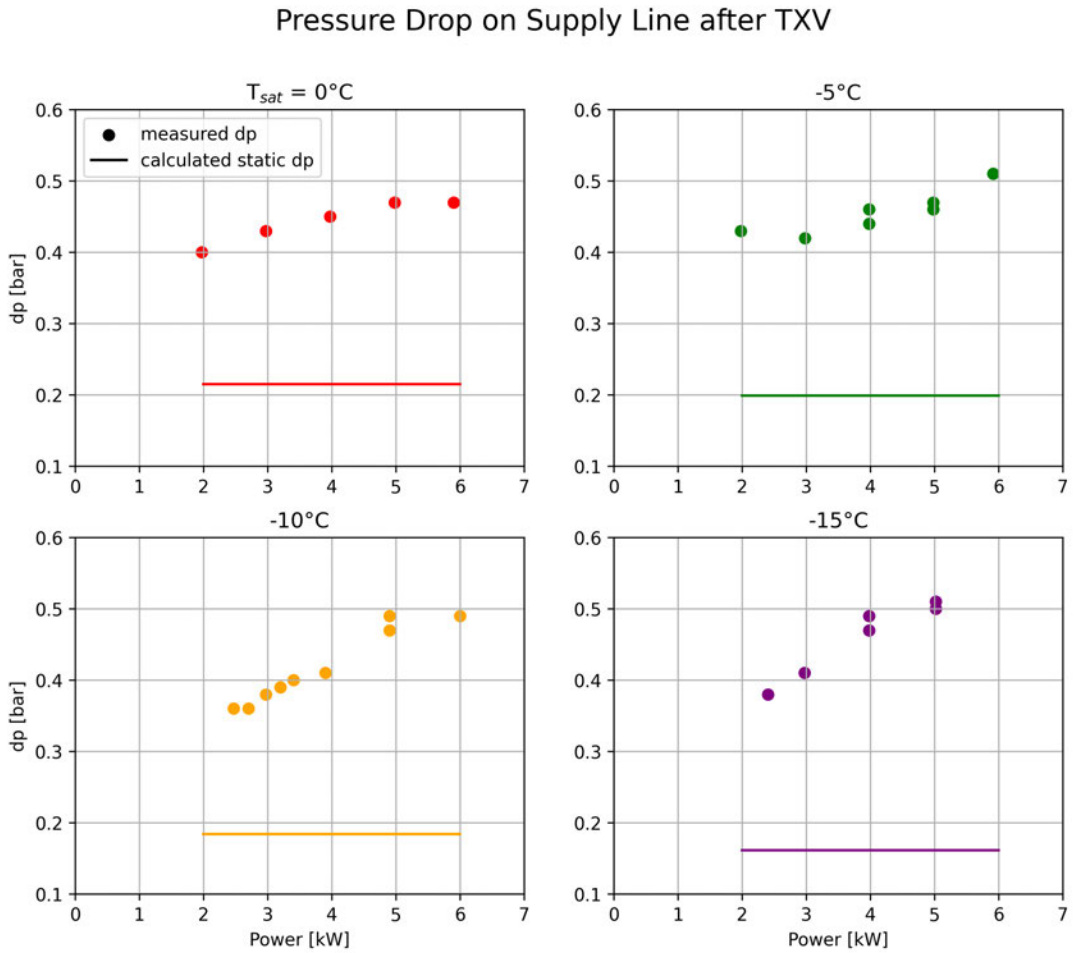

Figure 32: Two-phase pressure drop in vertical supply line and calculated static pressure drop for classification.

For the two lowest setpoints (-10°C, -15°C), the maximum compressor capacity is evident from the stagnation at 5 and 6 kW, indicating the setup's operational limits.

The static height contribution to the overall pressure drop is mostly less than 50 %. The two-phase carrying pipe is assumed adiabatic for the static Δp calculation, meaning no change in vapor quality along the length. The inlet conditions correspond to the receiver, thereby the density at the TXV outlet is obtained and further, the density is assumed to be uniform along the pipes.

However, like in the return line's single phase flow a quadratic relationship between Δp and heater power is expected. Given that the static height proportion is positive, the quadratic slope would approach the static height pressure drop at 0 kW.

Supply Line Saturated Liquid Pressure Drop The outlet of the condensing unit is saturated liquid. However, due to the 3 m height difference and frictional losses, a higher pressure drop occurs, causing the CO_2 to reach the TXV in a two-phase state with low vapor quality.

The TXV is positioned 3 m above the condensing unit and is located just before the double-shell structure begins, where only piping is permitted. Lowering its position would shift the pressure drop to the two-phase pipe, introducing additional capacity losses due to the heat leak of a longer pipe, outside the vessel's vacuum jacket.
Since the inlet pressure at the expansion valve was not measured, no further investigation can be done here.

5.6 Calculation of Velocities and Flow

In Chapter 3, an approximation of velocities is provided. The flows in the test setup are divided into two sorts, single-phase and two-phase flow. Pressure drop correlations allow for velocity or mass flux calculation. The following two sections provide a calculation of the return line velocity and the mass flux in the supply line after the TXV, using the following correlations:

- Return line velocities - Darcy Weisbach
- Supply line velocity after TXV - Friedel correlation

5.6.1 Return Line Velocities

The predicted velocities, align quite well with the results from the velocity calculation, as shown in Figure 33. Notable is the deviation at lower setpoints, as the velocities are calculated, form the pressure drop, to be higher, than the predicted values, using the enthalpy difference and density theoretically present after the expansion valve.
The lower the setpoint temperature of the fluid, the less accurate is the prediction by Darcy Weisbach. As the theoretical prediction assumes a constant superheat across the load variations, this might be a reason for deviation. Also the theoretical plot is not accounting for maximum compressor capacity, which is to see in plot -15°C where the velocity stagnates close to 10 m s^{-1}. In case of lower loads, <3 kW, the velocity falls below the specified minimum speed in horizontal pipes of 4 m s^{-1}. This is acceptable, since it is a vertical downward line and thus the oil transport is aided by gravity.

5.6.2 Supply Line Velocities

After TXV The results of the calculated mass fluxes are presented in Figure 34 in comparison with those derived from the theoretical calculation based on the enthalpy difference.
The pressure drop measured on the supply line after the TXV has three proportions, as mentioned in Section 2.5. As the Friedel correlation only considers the frictional pressure losses, the static dp proportion was subtracted beforehand. The pressure loss due to momentum was not considered here, as the inlet and outlet conditions were assumed to be equal for each calculation.

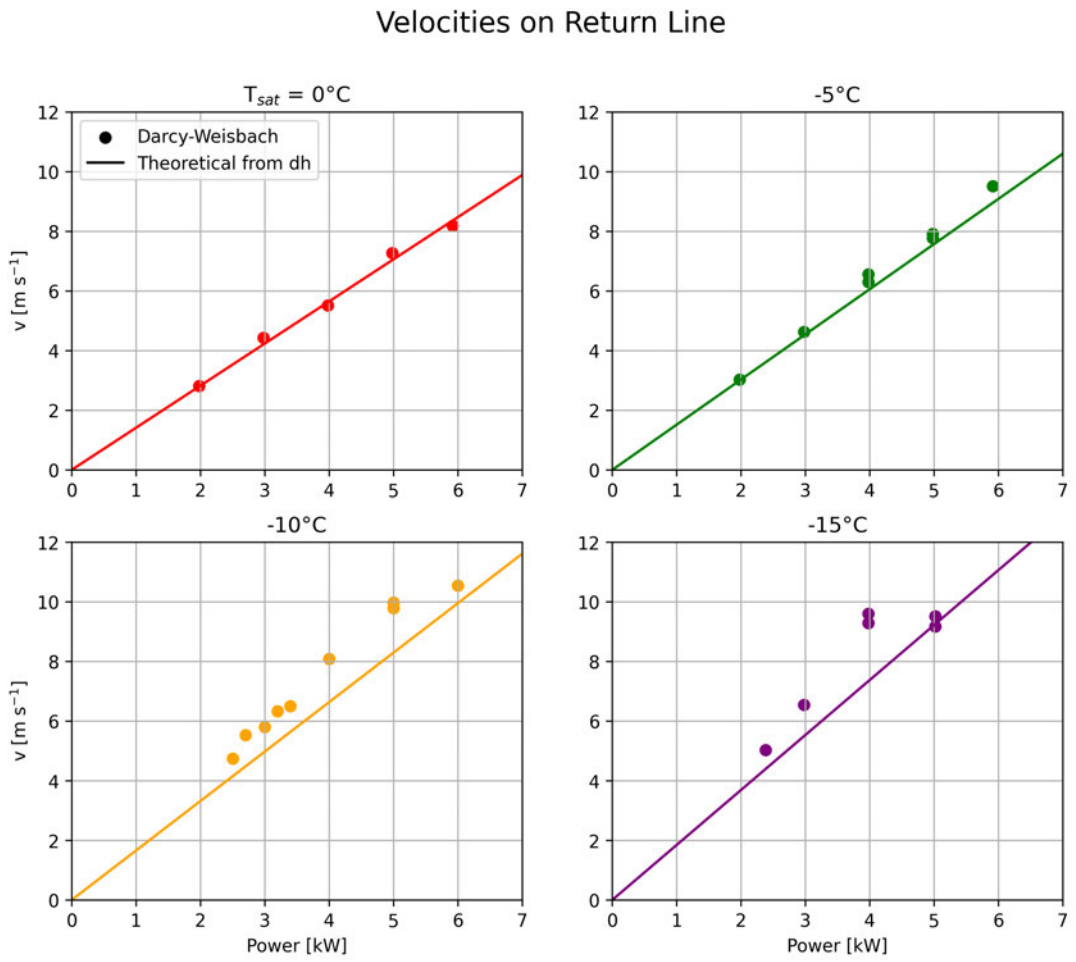

Figure 33: Return line velocities calculated from the measured pressure drop, compared to the theoretical prediction.

The results indicate a higher mass flux, than predicted by the theoretical calculations. This suggests that the pipe diameter accommodates the flow sufficiently across the tested load points and evaporation temperatures.

Similar to the observations in the pressure drop comparison, the increase of mass flux does not show a quadratic trend with power step-ups.

When comparing the results to the single-phase velocities calculated using the Darcy-Weisbach equation, the single-phase results align well with the theoretical predictions. However, the two-phase flow results deviate from the expected trend, suggesting that additional factors, such as phase interaction effects and non-uniform flow distribution, influence the observed behavior.

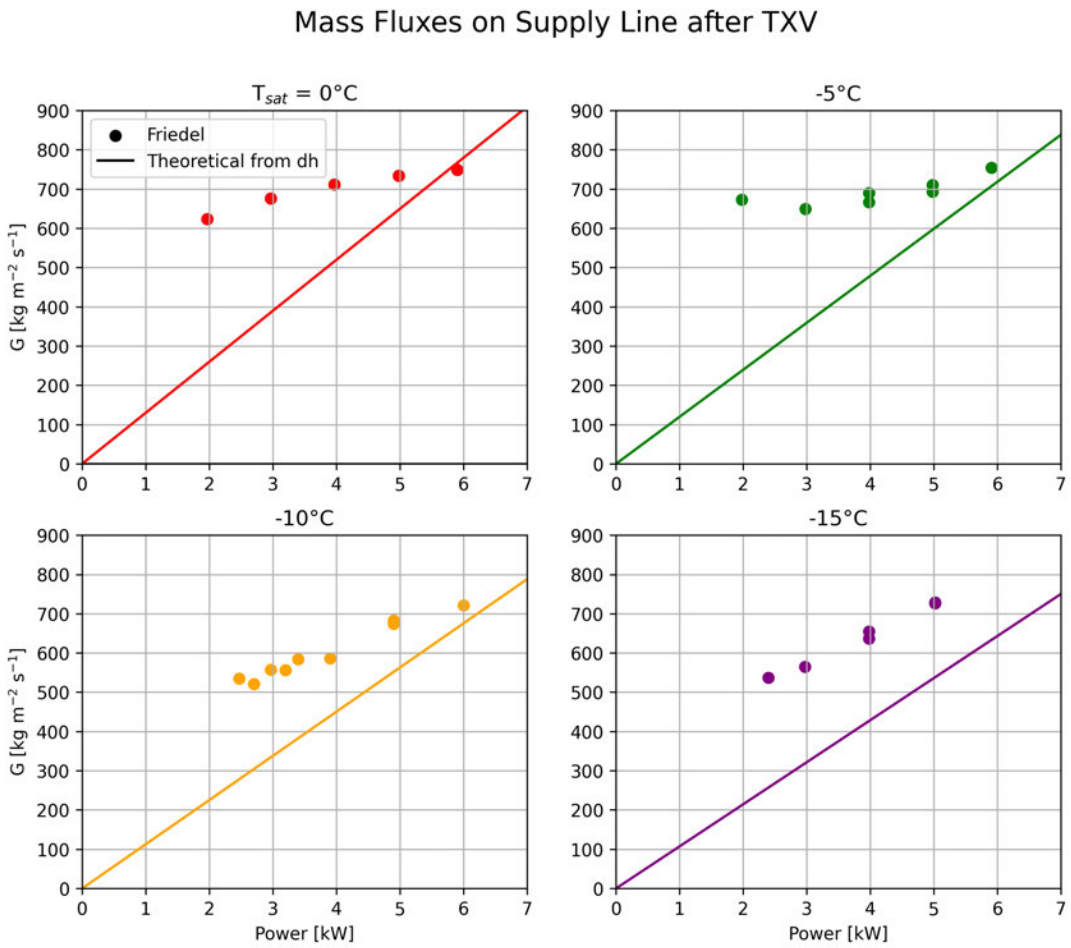

Figure 34: Comparison of theoretical mass flux and calculated from obtained measurements and Friedel correlation.

Liquid Line Before TXV The CO_2 in the supply line downstream of the TXV exits the condensing unit in saturated liquid state. The elevation of 3 m and the friction add to the pressure drop. However, the vapor quality is expected to be very low. A low void fraction can justify using the Darcy-Weisbach equation for a good approximation of the velocity. The density difference over the liquid supply line is small, another reason for single-phase approximation. Since the results of the returning vapor single-phase flow velocity calculation aligned well with the theoretical prediction using the enthalpy difference, it is here assumed, the prediction of the velocity in the liquid line is also adequate. This assumption is made due to the lack of monitored data.

6 Conclusions

This thesis explores the design and evaluation of a CO_2 storage vessel safety cooling system. The vessel is a semi-active component of the CO_2 cooling system for particle physics detectors, specifically designed for the Phase II upgrade of the LHC at CERN. The vessel disposes of pressure and temperature regulation via electrical heaters and the primary cooling system, a transcritical CO_2 vapor compression cycle.
In the event of primary system failure, the heat leak calculation elaborated the necessity of thermal management in order to maintain the service pressure and prevent refrigerant venting. The vessel's pressurization behavior is likely to differ from conventional models found in the literature, as the mixing effect of natural convection, which is enhanced by heat leaks from the thermosiphon piping, destroys the typical stratification, the layer formation by density. The result is claimed to be a uniform temperature distribution allowing for a more precise calculation of the pressurization time.
For the safety cooling system, a commercial condensing unit is chosen which will utilize a second heat exchanger mounted next to the primary cooling system. This approach, which is cooling by natural convection and avoiding direct fluid exchange, was not found in existing literature, except for accumulators in 2PACL systems.
The testing campaign led to the following key findings:

- The tests demonstrated the ability of the system to counteract heat leaks effectively. For higher load conditions, superheating adjustments can be made, as evidenced by the ground-level tests.
- The operational envelope from height setup tests was similar to the ground setup, indicating no significant performance loss.
- Oil return emerged as the primary bottleneck, but qualitative tests presented no evidence of faulty oil entrainment. The reduced pipe diameter likely aided the entrainment quality due to higher flow velocity.
- The pressure drop due to height and pipe length did not affect the setup's ability to meet the evaporation temperature setpoint, mirroring ground-level performance.
- The TXV did not limit system performance.
- The pipe diameter of 3/8" was sufficient, as theoretically predicted.
- The condensing unit's thermostat mode allows for operation based on real-time requirements.
- A proposed threshold for the pressure switch was found to be 42 bar with a 10% hysteresis, while the proposed switch offers an adjustment range of 5 to 50 bar.

Several limitations were identified:

- TXV tuning was conducted only at ground level and the TXV head was insulated, what might have reduced the maximum mass flow, due to the MOP charge of the bulb and the possibility of trapped liquid in proximity of the valve's diaphragm.
- The tests at height were only conducted using one charge, calculated after the manufacturer's instructions. Whether the system's performance in this specific application is

enhanced at a higher charge was not tested, as higher charges are noted to improve performance to an extent.
- The insulation of the two-phase pipe was not comparable to the evacuated perlite jacket used on the vessel, a better insulation will grant for a lower vapor quality at the evaporator inlet.
- While the pressure drop on the liquid supply line is inevitable, pressure measurements before expansion would provide more insight into the refrigerant's state before expansion.

6.1 Outlook

Future work could build upon these findings by exploring several key areas:

- Testing with original evaporator volume and ideally the planned design by SWEP, could offer further insights into performance and possibility of oil accumulation. Both the evaporator in this thesis and the planned evaporator are smaller than recommended by Danfoss, which can result in instabilities due to little thermal damping mechanism.
- Exploring alternative heat transfer mechanisms, such as air-blown systems or condensation, may provide more insights on the system's performance close to actual operating conditions.
- Testing superheat (SH) adjustment of the TXV during a height test could help optimize system's performance.
- Capillary testing at a fixed capacity is also recommended once a suitable heat load is specified.
- Investigation of the pressurization of the vessel due to the heat leak to verify the hysteresis of the pressure switch.
- Examination of the deviations between the mass flux predicted from the enthalpy difference and the calculated mass flux using the Friedel correlation.

This outlook provides a roadmap for further refinement of the safety cooling system design. Further investigations into the thermal behavior, pressure regulation, and oil management will enhance the reliability and efficiency of the system.

References

4.2 Thermal expansion valves (TEVs) - SWEP (2025). URL: https://www.swep.net/refrigerant-handbook/4.-expansion-valves/adf6/.

AG, Linde (n.d.). "Cryogenic Standard Tanks LITS 2". In: (). URL: https://assets.linde.com/-/media/global/engineering/engineering/home/products-and-services/plant-components/cryogenic-tanks/p_3_3_e_12_150dpi.pdf.

B.V, DENSO EUROPE (Nov. 2022). "Product Bulletin: Compressor oils and refrigerants". In: URL: www.denso-am.euwww.denso-am.co.uk.

Brown, Glenn O. (2002). "The history of the Darcy-Weisbach equation for pipe flow resistance". In: *Proceedings of the Environmental and Water Resources History*, pp. 34–43. DOI: 10.1061/40650(2003)4. URL: https://www.researchgate.net/publication/242138088_The_History_of_the_Darcy-Weisbach_Equation_for_Pipe_Flow_Resistance.

Christie, R J et al. (Aug. 2011). "Broad Area Cooler Concepts for Cryogenic Propellant Tanks 1". In: *2011 Thermal and Fluids Analysis Workshop (TFAWS)*.

Danfoss (2005). "Thermostatic expansion valves Fitters notes REFRIGERATION AND AIR CONDITIONING". In.

– (2021). *Micro Channel Heat Exchanger technology | A whole new level of system efficiency - YouTube*. URL: https://www.youtube.com/watch?v=mq454vJA0c8.

– (2023). *Danfoss Optyma™ Slim Pack | Deep-dive tour for experts - YouTube*. URL: https://www.youtube.com/watch?v=8528VR8LYi8.

Danfoss Refrigeration TXV (2025). URL: https://www.ptacsolutions.com/Danfoss-Refrigeration-067N9407-TXV-58ODF-x-1-18ODF-Straight-Body-60-Cap-Tube-R22R407C-Capacity--11-Ton-MOP-667-PSI-Ext-Equalized-number_p_205737.html.

Eames, Ian W., Adriano Milazzo, and Graeme G. Maidment (Feb. 2014). "Modelling thermostatic expansion valves". In: *International Journal of Refrigeration* 38 (1), pp. 189–197. ISSN: 01407007. DOI: 10.1016/J.IJREFRIG.2013.06.010.

Eikevik, Trygve Magne (2023). *CO2 Refrigeration Cycle and Systems*. Ed. by Xin-Rong Zhang and Trygve Magne Eikevik. Vol. 96. Springer International Publishing. ISBN: 978-3-031-22511-6. DOI: 10.1007/978-3-031-22512-3. URL: https://link.springer.com/10.1007/978-3-031-22512-3.

Hallewell, G D (2023). "The "green" use of fluorocarbons in Cherenkov detectors and silicon tracker cooling systems: challenges and opportunities in an unfolding era of alternatives". In: *Eur. Phys. J. Plus* 138, p. 1141. DOI: 10.1140/epjp/s13360-023-04703-w. URL: https://doi.org/10.1140/epjp/s13360-023-04703-w.

Honert A. van den Reactor Centrum Nederland, Petten (Netherlands) (Dec. 1969). *Pressurizer Dynamics Response to Load Transients. RCN Report*.

Ikeda, Harutomo et al. (2004). "Purdue University Purdue e-Pubs International Refrigeration and Air Conditioning Conference School of Mechanical Engineering 2004 International Refrigeration and Air Conditioning Conference at Purdue". In: URL: http://docs.lib.purdue.edu/iracc/680.

Inc., Cashco (Jan. 2017). *Storage Tank Venting Solution - YouTube*. URL: https://www.youtube.com/watch?v=eLdnFCUF2jk&t=4s.

Inc., Cashco (n.d.). “TECHNICAL BULLETIN Tank Blanketing Valve”. In: (). URL: https://www.cashco.com/amfile/file/download/file/253/product/25238/.

Kadish, Shai et al. (Feb. 2022). “Computer Vision-Based Classification of Flow Regime and Vapor Quality in Vertical Two-Phase Flow”. In: *Sensors* 22 (3). ISSN: 14248220. DOI: 10.3390/S22030996.

Karnaz, Joseph Anthony (2022). “What’s Important When Designing For A New Refrigerant? Lubricant Perspective”. In: URL: https://docs.lib.purdue.edu/iracc.

Lang, Stephan et al. (2016). “Thermal Conductivity of Vacuum Insulation Materials for Thermal Energy Stores in Solar Thermal Systems”. In: *Energy Procedia*. Vol. 91. Elsevier Ltd, pp. 172–181. DOI: 10.1016/j.egypro.2016.06.196.

Li, H et al. (2002). *Field And Laboratory Evaluations Of Lubricants For CO2 Refrigeration*. URL: http://docs.lib.purdue.edu/iracc/581.

Li, Zhengqing et al. (Nov. 2023). “A new method for evaluating the heat leak of cryogenic vessels without exhaust gas”. In: *Heliyon* 9 (11). ISSN: 24058440. DOI: 10.1016/j.heliyon.2023.e21370. URL: http://www.cell.com/article/S240584402308578X/fulltext%20http://www.cell.com/article/S240584402308578X/abstract%20https://www.cell.com/heliyon/abstract/S2405-8440(23)08578-X.

Lin, C.-S., N. T. Vandresar, and M. M Hasan (1991). “A pressure control analysis of cryogenic storage systems”. In.

Nunez, Emerson Escobar et al. (2008). “Tribological study comparing pag and poe lubricants used in air-conditioning compressors under the presence of co2”. In: *Tribology Transactions* 51 (6), pp. 790–797. ISSN: 1547397X. DOI: 10.1080/10402000801911861. URL: https://www.researchgate.net/publication/245314695_Tribological_Study_Comparing_PAG_and_POE_Lubricants_Used_in_Air-Conditioning_Compressors_under_the_Presence_of_CO2.

Optyma™ iCO2 condensing units - R744 | 50 Hz (2023). URL: https://assets.danfoss.com/documents/latest/297116/AB399636244436en-000203.pdf.

Perry, Wayne (Oct. 2018). “The Basics of Rotary Screw Compressor Lubricants”. In.

Plachta, D W, W L Johnson, and J R Feller (2015). “ZERO BOIL-OFF SYSTEM TESTING”. In.

Schmid, David et al. (June 2022). “Adiabatic two-phase pressure drop of carbon dioxide in different channel orientations”. In: *International Journal of Heat and Fluid Flow* 95, p. 108966. ISSN: 0142-727X. DOI: 10.1016/J.IJHEATFLUIDFLOW.2022.108966.

Schmidt, Burkhard (Apr. 2016). “The High-Luminosity upgrade of the LHC: Physics and Technology Challenges for the Accelerator and the Experiments”. In: *Journal of Physics: Conference Series* 706 (2), p. 022002. ISSN: 1742-6596. DOI: 10.1088/1742-6596/706/2/022002. URL: https://iopscience.iop.org/article/10.1088/1742-6596/706/2/022002%20https://iopscience.iop.org/article/10.1088/1742-6596/706/2/022002/meta.

Statements: Capacity Rating of Expansion Valves - ASERCOM (n.d.). URL: https://www.asercom.org/statements/.

Sunu, Putu Wijaya et al. (Feb. 2018). “Capillary Tube and Thermostatic Expansion Valve Comparative Analysis in Water Chiller Air Conditioning”. In: *Journal of Physics: Conference Series* 953 (1). ISSN: 17426596. DOI: 10.1088/1742-6596/953/1/012063.

Tang, Chuhao, Zhanfeng Huang, and Tingxun Li (Nov. 2024). “Visualization Study on Oil Return Characteristics of Vapor Compression Heat Pump System”. In: *Energies* 17 (21). ISSN: 19961073. DOI: 10.3390/EN17215299. URL: https://www.researchgate.net/publication/385264613_Visualization_Study_on_Oil_Return_Characteristics_of_Vapor_Compression_Heat_Pump_System.

The accelerator complex | CERN (2025). URL: https://home.cern/science/accelerators/accelerator-complex.

Thermostatic expansion valve type TE2 for R744; Thermostatic expansion valve type TE2 for R744 (2023). URL: https://assets.danfoss.com/documents/317336/AI394975009003en-000202.pdf.

Thome, John R (n.d.). *Engineering Data Book III*. URL: http://ltcm.epfl.ch.

Tropea, P. et al. (Aug. 2019). “Advancements and plans for the LHC upgrade detector thermal management with CO2 evaporative cooling”. In: *Nuclear Instruments and Methods in Physics Research Section A: Accelerators, Spectrometers, Detectors and Associated Equipment* 936, pp. 644–645. ISSN: 0168-9002. DOI: 10.1016/J.NIMA.2018.10.083.

Verlaat (Sept. 2023). *ITk Surface Storage design approach*.

Verlaat, B, A Van Lysebetten, and M Van Beuzekom (2008). “CO2 cooling for HEP experiments”. In: DOI: 10.5170/CERN-2008-008.328. URL: https://cds.cern.ch/record/1158652.

Verlaat, Bart and Auke-Pieter Colijn (2009). “CO 2 Cooling Developments for HEP Detectors”. In: *VERTEX 2009*.

Verlaat, Bart, Paolo Petagna, et al. (Aug. 2019). “CO2 cooling challenges at CERN for the future phase 2 upgrade program”. In: *Refrigeration Science and Technology* 2019-August, pp. 351–359. ISSN: 01511637. DOI: 10.18462/IIR.ICR.2019.1690. URL: https://cds.cern.ch/record/2723848.

Vijayan, P.K. and A.K. Nayak (2005). *Natural circulation in water cooled nuclear power plants : phenomena models and methodology for system reliability assessments*. International Atomic Energy Agency, pp. 89–99. ISBN: 920110605X. URL: https://inis.iaea.org/collection/NCLCollectionStore/_Public/37/032/37032143.pdf?r=1.

Where to mount the TXV sensing bulb? (2025). URL: https://abrwholesalers.com/blog/post/txv.

Yoshioka, Shun, Hyunyoung Kim, and Kazushige Kasai (May 2008). *Effect of PAG oil circulation rate on the heat transfer performance of air-cooled heat exchanger in carbon dioxide heat pump system*. Tech. rep. 9 th International IEA Heat Pump Conference. URL: https://etkhpcorderapi.extweb.sp.se/api/file/897.

Zwalinski, L. et al. (Feb. 2023). “Elsevier B.V. : Progress in new environmental friendly low temperature detector cooling systems development for the ATLAS and CMS experiments”. In: *Nucl. Instrum. Methods Phys. Res., A* 1047, p. 167688. ISSN: 01689002. DOI: 10.1016/J.NIMA.2022.167688. URL: https://cds.cern.ch/record/2882584.

Hochschule für Angewandte Wissenschaften Hamburg
Hamburg University of Applied Sciences

Erklärung zur selbstständigen Bearbeitung einer Abschlussarbeit

Gemäß der Allgemeinen Prüfungs- und Studienordnung ist zusammen mit der Abschlussarbeit eine schriftliche Erklärung abzugeben, in der der Studierende bestätigt, dass die Abschlussarbeit „– bei einer Gruppenarbeit die entsprechend gekennzeichneten Teile der Arbeit [(§ 18 Abs. 1 APSO-TI-BM bzw. § 21 Abs. 1 APSO-INGI)] – ohne fremde Hilfe selbständig verfasst und nur die angegebenen Quellen und Hilfsmittel benutzt wurden. Wörtlich oder dem Sinn nach aus anderen Werken entnommene Stellen sind unter Angabe der Quellen kenntlich zu machen."

Quelle: § 16 Abs. 5 APSO-TI-BM bzw. § 15 Abs. 6 APSO-INGI

Dieses Blatt, mit der folgenden Erklärung, ist nach Fertigstellung der Abschlussarbeit durch den Studierenden auszufüllen und jeweils mit Originalunterschrift als letztes Blatt in das Prüfungsexemplar der Abschlussarbeit einzubinden.
Eine unrichtig abgegebene Erklärung kann -auch nachträglich- zur Ungültigkeit des Studienabschlusses führen.

Erklärung zur selbstständigen Bearbeitung der Arbeit

Hiermit versichere ich,

Name: _____

Vorname: _____

dass ich die vorliegende – bzw. bei einer Gruppenarbeit die entsprechend gekennzeichneten Teile der Arbeit – mit dem Thema:

ohne fremde Hilfe selbständig verfasst und nur die angegebenen Quellen und Hilfsmittel benutzt habe. Wörtlich oder dem Sinn nach aus anderen Werken entnommene Stellen sind unter Angabe der Quellen kenntlich gemacht.

- die folgende Aussage ist bei Gruppenarbeiten auszufüllen und entfällt bei Einzelarbeiten -

Die Kennzeichnung der von mir erstellten und verantworteten Teile der ist erfolgt durch:

[redacted]

_____ _____ _____
Ort Datum Unterschrift im Original